TOPICAL REVIEW

Interatomic Coulombic electron capture: the story so far

IOP Publishing Journal of Physics B: Atomic, Molecular and Optical Physics

J. Phys. B: At. Mol. Opt. Phys. **56** (2023) 232001 (19pp) https://doi.org/10.1088/1361-6455/ad073c

Topical Review

Interatomic Coulombic electron capture: the story so far

Annika Bande[1,2], Elke Fasshauer[3,4,5], Axel Molle[6], Daniel Peláez[7], Federico M Pont[8,10] and Nicolas Sisourat[9,*]

[1] Leibniz University Hannover, Institute of Inorganic Chemistry, Callinstr. 9, 30167 Hannover, Germany
[2] Theory of Electron Dynamics and Spectroscopy, Helmholtz-Zentrum Berlin für Materialien und Energie GmbH, Hahn-Meitner-Platz 1, 14109 Berlin, Germany
[3] Institute of Physical and Theoretical Chemistry, University of Tübingen, Auf der Morgenstelle 18, 72076 Tübingen, Germany
[4] LISA$^+$, University of Tübingen, Auf der Morgenstelle 15, 72076 Tübingen, Germany
[5] Department of Chemistry, University of Oxford, Oxford OX1 3QZ, United Kingdom
[6] Institute for Theoretical Physics, Department of Physics and Astronomy, KU Leuven, 3001 Leuven, Belgium
[7] Université Paris-Saclay, CNRS, Institut des Sciences Moléculaires d'Orsay, 91405 Orsay, France
[8] Facultad de Matemática, Astronomía, Física y Computación, Universidad Nacional de Córdoba, Ciudad Universitaria, Córdoba X5000HUA, Argentina
[9] Sorbonne Université, CNRS, Laboratoire de Chimie Physique Matière et Rayonnement, UMR 7614, F-75005 Paris, France
[10] Instituto de Física Enrique Gaviola, CONICET-UNC, Ciudad Universitaria, Córdoba X5000HUA, Argentina

E-mail: Nicolas.Sisourat@sorbonne-universite.fr

Received 26 June 2023, revised 2 October 2023
Accepted for publication 26 October 2023
Published 13 November 2023

Abstract

Inter-particle Coulombic electron capture (ICEC) is an environment-enabled electron capture process by means of which a free electron can be efficiently attached to a system (e.g. ion, atom, molecule, or quantum dot (QD)). The excess electron attachment energy is simultaneously transferred to a neighbouring system which concomitantly undergoes ionization (or excitation). ICEC has been theoretically predicted in van-der-Waals and in hydrogen-bonded systems as well as in QD arrays. The theoretical approaches employed in these works range from analytical models to electronic structure and (quantum) dynamical calculations. In this article, we provide a comprehensive review of the main theoretical approaches that have been developed and employed to investigate ICEC and summarize the main conclusions learned from these works. Since knowledge on ICEC is still in its early stage, we conclude this review with our own views and proposals on the future perspectives for the research in ICEC.

Keywords: electron attachment, interparticle Coulombic electron capture, clusters

(Some figures may appear in colour only in the online journal)

* Author to whom any correspondence should be addressed.

1. Introduction

Electron attachment is a fundamental process of great importance in many areas of basic and applied science. It plays a central role in astrophysics [1, 2], plasma physics [3], and accelerator physics [4]. Furthermore, it underlies the reduction and oxidation properties of matter and thus it is also of relevance to electrochemistry [5, 6], photochemistry [7], high-energy chemistry [8], biology [9] as well as to novel applications of solid state devices [10, 11].

Electron attachment to atoms, molecules and clusters has been investigated for decades (see e.g. the Reviews [12, 13] and papers of this special issue). Gas-phase electron capture processes are well understood from diverse experiments as well as from theoretical investigations (see [14] and references therein). However, in clusters and even more so in condensed phase, the nature of these reactions is still an open field of research. We address in this review one of the possible electron capture processes, namely the inter-particle Coulombic electron capture (ICEC), which takes place only in systems embedded in a environment.

ICEC is a process in which a free electron can efficiently attach to an acceptor A (i.e. ion, atom, molecule, quantum dot (QD), etc). The excess attachment energy is transferred to a neighbouring system B which gets ionized (or excited),

$$e(\varepsilon) + A + B \rightarrow A^- + B^+ + e(\varepsilon'). \tag{1}$$

The ICEC process exists in several variants. If the excess energy is used to ionize the neighbour, which emits the so-called ICEC electron, then the process is called direct ICEC (see figure 1). This naming is independent of whether the electron is captured into the lowest possible orbital (figure 1(a)) or into an energetically higher-lying orbital (figure 1(b)). In the latter case, the system subsequently relaxes via photon emission or via another environmentally assisted pathway.

It is also possible that the transferred excess energy is used to create a resonance state, i.e. a bound state in the continuum. This process is therefore called resonant ICEC. The resonance state can subsequently relax under emission of a photon, which is alternatively also discussed in the research literature as *two-centre dielectronic recombination* [16–19]. Hence the process is considered as an inverse process to a resonant inter-particle Coulombic decay (ICD) [20], see figure 2(a). We note, that the latter process has also been considered for positron attachment [21]. Another possibility is that the resonance state relaxes by transferring the excess energy to a third site, which is ionized [22]. Alternatively, it can undergo a participator resonant ICD upon emission of an electron, if the electron was initially captured into an electronically excited state (figure 2(b)).

In contrast to the delocalized nature of the resonance state in the resonant ICEC process, it is also possible to create a resonance state localized on A, if the initial kinetic energy of the captured electron matches an internal energy difference of this unit (see figure 3). This resonance state can then decay via several pathways, e.g. a participator resonant ICD illustrated in figure 3(a) or a spectator resonant ICD shown in figure 3(b). Due to its initiation by a two-electron process on unit A this process is called dielectronic ICEC. The analogue process in photorecombination [23] at a single site was observed in the case of dielectronic recombination of isolated cations induced by capture into a Rydberg state [24]. For every single process in the above manifold, energy conservation is required.

ICEC was discovered through analytical scattering theory [19, 20, 25]. Indeed, it was shown that the ICEC process led to a strong enhancement of the electron attachment (or capture) cross sections compared to isolated A. This was demonstrated in several systems such as Ne^+ surrounded with Xe atoms or benzene (Bz) molecules, He^+ in the presence of Ar and Bz, or the Mg^+-Br^- system [20, 25].

As such, ICEC constitutes an efficient process for reducing a species while oxidizing one of its neighbours. It should be noted that the two species involved in ICEC may have different ionization potentials thus enabling the modulation of the energy of the ICEC electron. Such electrons, typically of a few electron-Volts of kinetic energy, are known to be highly genotoxic, because they can undergo dissociative electron attachment (DEA) of biomolecules [26–28]. Note that the cross section for DEA strongly depends on the kinetic energy of the free electron. ICEC might thus be a general process underlying the damage of living cells under ionizing radiation as well as a major actor in the electron-mediated chemistry which leads to the formation of pre-biotic species in interstellar environments.

It is fair to say that the research field of ICEC is just at its infancy. Indeed, including the initial works in which scattering theory was applied to describe the most fundamental ICEC processes, all of the ICEC mechanisms described so far have been discovered from a purely theoretical perspective. As a result of this, various theoretical methods and approximations have been developed to account for the very different nature of the systems prone to exhibit any (or several) of the ICEC pathways. The first aim of this review is to present a global overview of the different ICEC processes together with an introduction to the different classes of materials and systems for which ICEC was found to be relevant. This is followed by a detailed summary of the main conclusions learned from these works. We conclude this review with our own point of view on the perspectives for the largely unexplored research field of ICEC.

2. ICEC between two distant partners

In order to be observable, the environment-assisted electron capture needs to fulfil energy conservation and to be at least as efficient as the normal photo-recombination. This efficiency is characterized by the cross section of the process, which gives the probability of an incoming electron with wavevector k being captured and an electron with wavevector k' being emitted. For a general inelastic scattering event involving several channels, the cross section reads [29]:

$$\sigma_{\mathrm{ICEC}}(k) = \frac{1}{g_{\mathrm{in}}} \sum_{\mathrm{in,out}} \int \frac{\mathrm{d}\Omega_{\mathbf{k}}}{4\pi} \int \mathrm{d}\Omega_{\mathbf{k}'} \frac{m_e^2}{(2\pi\hbar^2)^2} \frac{k'}{k} \left|T(\mathrm{out} \leftarrow \mathrm{in})\right|^2. \tag{2}$$

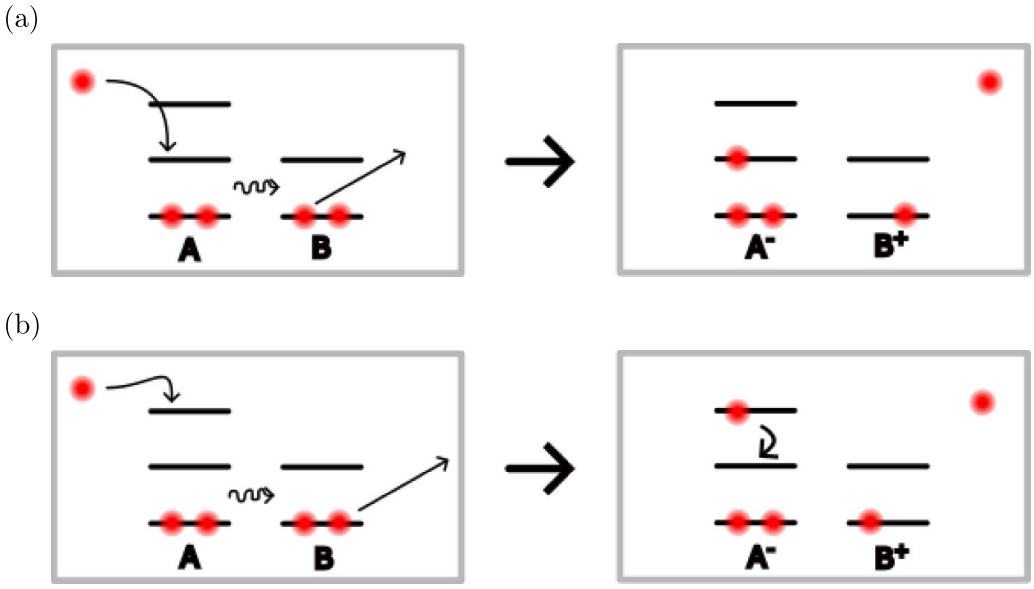

Figure 1. Direct ICEC processes. Reproduced from [15]. CC BY 4.0.

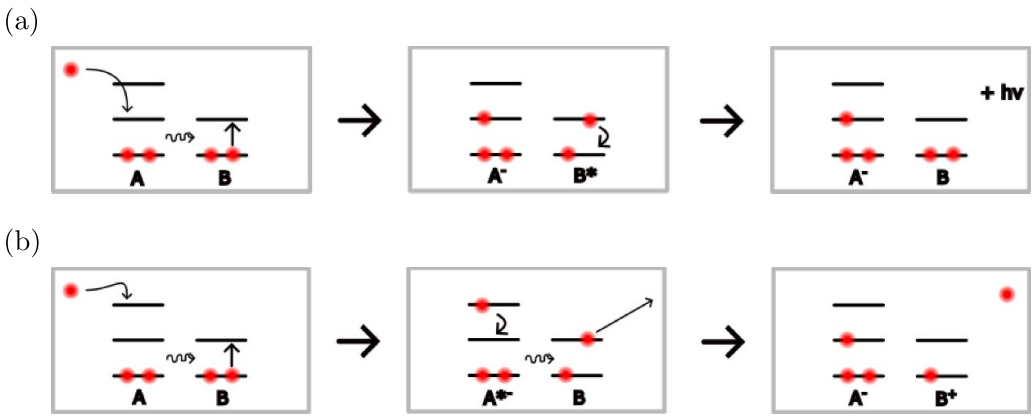

Figure 2. Resonant ICEC processes. Reproduced from [15]. CC BY 4.0.

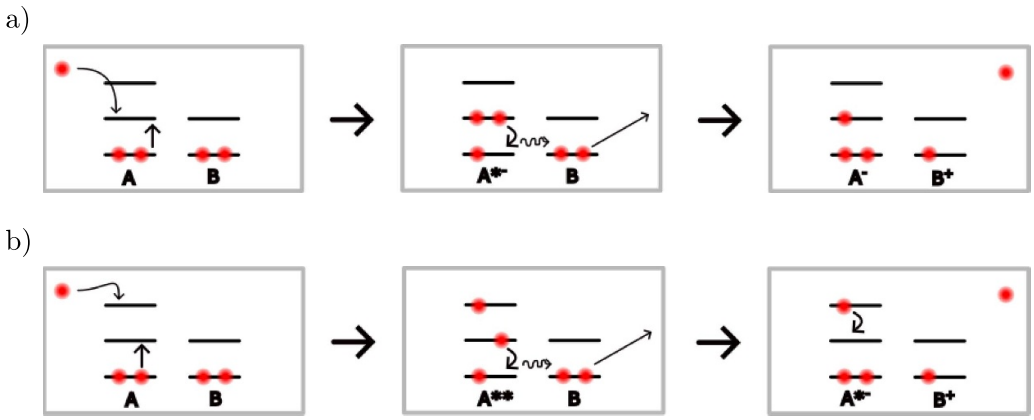

Figure 3. Dielectronic resonance-enhanced ICEC processes. Reproduced from [15]. CC BY 4.0.

Here, the scattering T-matrix describes the interaction between the two (appropriately normalized) continuum states, the total cross section includes contributions from all incoming and outgoing channels, the integration over the solid angles of the incoming and outgoing electrons $\Omega_{\mathbf{k}}$ and $\Omega_{\mathbf{k}'}$, respectively, ensures that all possible spatial directions are taken into account and the multiplicity of the initial state g_{in} averages over all possible initial states and thereby normalizes

the cross section to the interaction with a single incoming electron.

This expression of the cross section can be simplified for systems with weakly interacting units. In such cases, it is possible to estimate the cross section directly from the intrinsic properties of the units as well as their geometry [25]. Furthermore, the long-range Coulomb interaction between electrons on the different sites moderates the energy transfer through space, which according to quantum field theory is the transfer of a virtual photon [30].

These estimates allow us to understand, how the cross section is influenced by the different system parameters and can guide the choice of systems for both numerical simulations and experiments. From a historical perspective, the asymptotic estimates were the first evidence for the existence of ICEC.

In the following, we summarize the energy balance condition, the derivation of the cross section estimate, i.e. the asymptotic approximation, what we can learn from it and how it impacts the ICEC efficiency in different systems.

2.1. Asymptotic approximation

Our aim here is to describe the ICEC process for two separate and weakly interacting units (A and B). In this context, we speak of the *asymptotic regime* and the *asymptotic approximation* when sites A and B are sufficiently separated such that their interaction causes an only marginal disturbance of the units' wavefunctions and their individuality can be asserted. In this case and based on the energies long before the incoming electron interacts with our system AB and long after the emitted electron has left it, the energy balance involves the kinetic energy of the captured and emitted electrons at infinite distance ε and ε' as well as the electron affinity $\mathrm{EA}^{(\mathrm{A})}$ of A and the ionization potential $\mathrm{IP}^{(\mathrm{B})}$ of B as [20, 25]:

$$\mathrm{EA}^{(A)} + \varepsilon = \mathrm{IP}^{(B)} + \varepsilon' = h\nu. \tag{3}$$

Here, $h\nu$ represents the transferred energy.

When considering ICEC in this spirit, as a virtual photon mechanism, the entire process can be rationalized in terms of cross sections for the intermediate steps, as it is the case for the ICD asymptotic equation [31–33]. Due to the weak interaction between the units, it is possible to use first order perturbation theory in equation (2). In this way, the wavefunction can be expressed as the product of the wavefunction for the incident electron adhering to incoming boundary conditions (+) plus unit A and the wavefunction of unit B, including the electron emitted during the process adhering to outgoing boundary conditions (−) for the initial and final state:

$$|\mathbf{k}; \Phi_{\mathrm{AB}}+\rangle = |\mathbf{k}; \Phi_{\mathrm{A}}+\rangle |\Phi_{\mathrm{B}}\rangle \tag{4}$$

$$|\mathbf{k}'; \Phi_{\mathrm{A^-B^+}}-\rangle = |\Phi_{\mathrm{A^-}}\rangle |\mathbf{k}'; \Phi_{\mathrm{B^+}}-\rangle. \tag{5}$$

Consequently, the smaller the overlap of the partners' wavefunctions are, i.e. the further the partners are apart, the better this approximation becomes. It is therefore called the asymptotic approximation. The overlap is strictly depending on and characteristic of the different systems.

Using this product wavefunction, the Coulomb interaction between charges located on A with charges on B functions as a perturbation operator. Performing a multipole expansion on this Coulomb interaction, truncation after the dominant term, and application of the principle of detailed balance [34] yields

$$\sigma_{\mathrm{ICEC},i}(\varepsilon) = \frac{3(\hbar c)^4}{4\pi} \frac{\sigma_{\mathrm{PI}}^{(\mathrm{B})}(\varepsilon')}{R^6 (h\nu_i)^4} \sigma_{\mathrm{PR}}^{(\mathrm{A})}(\varepsilon), \tag{6}$$

as cross section for a single direct ICEC channel i of a single AB pair. This expression can be attributed to the interaction between dipoles located at the two involved partners. Here, $\sigma_{\mathrm{PR}}^{(\mathrm{A})}(\varepsilon)$ is the photo-recombination cross section of A, $\sigma_{\mathrm{PI}}^{(\mathrm{B})}(\varepsilon')$ is the photoionization cross section of B, and R is the distance between A and B.

As can directly be seen from equation (6), ICEC dominates over photo-recombination for a specific channel, whenever the prefactor to the photo-recombination cross section exceeds unity. In decreasing priority, this is the case when:

1. the **partners are in proximity**. Hence, a small interparticle distance R increases the probability for an ICEC process. However, for a system-dependent small interparticle distance, the asymptotic cross section in equation (6) becomes a lower bound and more accurate methods become necessary for an accurate description of ICEC.
2. the **transferred energy $h\nu$ is low**. Both a slow incoming electron and a weak potential capturing the electron related to the electron affinity are favourable for the observation of ICEC.
3. the **ionization cross section of B is high**.

Since cross sections are additive, the total ICEC cross section is then given by the sum over all individual ICEC channel contributions $\sigma_{\mathrm{ICEC}} = \sum_i \sigma_{\mathrm{ICEC},i}$. Not only does the energetic accessibility of several ICEC channels increase the total ICEC cross section, but it also increases the probability to have one channel with a particularly high ICEC cross section where only a comparatively small amount of energy is transferred between the partners as illustrated in figure 1(b).

An ICEC channel is characterized by the capturing and emitting states as well as by the electron emitting partner. Hence, within the asymptotic approximation and under the assumption of distinguishable partners, the total ICEC cross section scales linearly with the number of equivalent and equidistant partners N.

In the case of the dielectronic resonance-enhanced ICEC processes depicted in figure 3 with the localized electron capture process, an asymptotic expression can straightforwardly be deduced [20]:

$$\sigma_{d\mathrm{ICEC}} = \frac{\pi}{k^2} \frac{g_d}{g_{in}} \frac{\Gamma_{\mathrm{PR}}\Gamma_{\mathrm{ICD}}}{(\varepsilon - \varepsilon_R)^2 + \Gamma^2/4}. \tag{7}$$

Here, g_d and g_{in} are the weights of the decaying and the initial state, respectively, $\mathbf{k}$ is the absolute wave vector of the incident electron, and ε_R is the energy of the decaying state.

The successive electron capture and electronic decay via resonant ICD (RICD) processes of a single ICEC pathway

imprints the characteristic Lorentzian line shape of an electronic decay process on equation (7). Its width is hereby given by the total decay width Γ, which constitutes the sum over the decay width of all possible decay mechanisms including ICD, photo-recombination and autoionization [35]. The signal is scaled by the RICD decay width Γ_{ICD} as well as the photo-recombination decay width Γ_{PR}. Most notably, the ICD width is usually several orders of magnitude larger than the photo-recombination width. If no other pathways are energetically accessible, the total width can be approximated to the ICD width ($\Gamma \approx \Gamma_{\mathrm{ICD}}$). In this scenario and when the kinetic energy of the incident electron ε matches the resonance energy ε_R, the cross section is significantly enhanced by this dielectronic pathway, as can be seen from equation (7).

If an autoionization process is energetically allowed, its decay width is usually of the same order of magnitude than an ICD width. Since it enters equation (7) via the total decay width in the denominator, the larger the autoionization width, the smaller is the ICEC cross section.

Furthermore, a dielectronic resonance-enhanced ICEC process is most probable, when the multiplicity of the capturing state (g_d) is higher than the one of the initial state (g_{in}), and when the incident electron energy fits well with a resonance of unit A. Moreover, deduced from the asymptotic approximation of the ICD decay width, the ICEC cross section is high, when both the transition dipole moment on unit A as well as the ionization cross section of unit B are high. Additionally, and as for the direct ICEC case, a ν^{-4}-dependence benefits small virtual photon energies whereas the R^{-6} dependence favours close partners.

In order to assess nano-sized components performing ICEC, the so-called ICEC radius R_{ICEC} was recently defined as the distance at which ICEC and photo-recombination are equally efficient [36]. Its working expressions were deduced from the asymptotic ICEC cross section in equation (6) utilizing the fact that the cross section in this approximation does not carry any information about the system size. For a single pair and channel i, this distance is given by [36]

$$R_{\mathrm{ICEC},i} = \left(\frac{3\,(\hbar c)^4}{4\pi} \frac{\sigma_{\mathrm{PI}}^{(\mathrm{B})}\left(\varepsilon_i'\right)}{\left(h\nu_i\right)^4} \right)^{\frac{1}{6}}. \tag{8}$$

$R_{\mathrm{ICEC},i}$ is a quantity more easily comparable across experiments and theoretical systems by taking the free variable parameter of intermolecular distance R out of the equation as

$$\sigma_{\mathrm{ICEC},i} R_i^6 = \sigma_{\mathrm{PR}}^{(\mathrm{A})} R_{\mathrm{ICEC},i}^6, \tag{9}$$

which has successfully been applied to different systems and degrees of theory since (cf discussion in section 3.3) [37]. With its definition, the ICEC radius is on equal footing to the closely related field of Förster resonance energy transfer (FRET). Its respective parameter, the Förster radius, provides an evaluation of the reach of the long-range energy transfer for a specific system and incident energy.

Analogue to the FRET quantum yield, which indicates the probability of FRET to occur after excitation by one photon, the ICEC efficiency can be defined as [36]

$$\eta_{\mathrm{ICEC}} = \frac{R_{\mathrm{ICEC}}^6}{R^6 + R_{\mathrm{ICEC}}^6}. \tag{10}$$

Considering the possibility of multiple ICEC and photo-recombination channels, the individual contributions should be combined in a weighted sum to yield the total ICEC radius [36]

$$R_{\mathrm{ICEC}}\left(\varepsilon\right) = \frac{3\,(\hbar c)^4}{4\pi} \sum_i w_{i,\varepsilon} \frac{\sigma_{\mathrm{PI}}^{(\mathrm{B})}\left(\varepsilon_i'\right)}{\left(h\nu_{i,\epsilon}\right)^4}. \tag{11}$$

Here, multiple channels, each of which becomes energetically available at different incident electron energies, have been included.

The ICEC radius is expected to be of significance to evaluate theoretical and experimental systems since it directly relates to the product of the amplification factor $(\sigma_{\mathrm{ICEC}}/\sigma_{\mathrm{PR}})$, and the respective interatomic distance R to the sixth power which can be shown—for each individual capture channel, i, at the same time as for the collective sum of contributions from all available capture channels to the overall ICEC—to be:

1. limited in magnitude from above by quantity R_{max} for all incident energies as

$$\frac{\sigma_{\mathrm{ICEC}}}{\sigma_{\mathrm{PR}}} R^6 = R_{\mathrm{ICEC},i}^6 \leqslant R_{\mathrm{max}}^6 = \frac{3\,(\hbar c)^4}{4\pi} \max_{\epsilon} \left[\frac{\sigma_{\mathrm{PI}}^{(\mathrm{B})}\left(\epsilon\right)}{\epsilon^4} \right], \tag{12}$$

   which can be estimated exclusively from the accessible photoionization cross section of the assisting partner; and
2. predictable in its large-energy behaviour (where $\epsilon \gg \mathrm{EA}^{(A)}$ in equation (3)) converging to the captor-independent distance R_∞ as function of incident energy ϵ:

$$\frac{\sigma_{\mathrm{ICEC}}}{\sigma_{\mathrm{PR}}} R^6 = R_{\mathrm{ICEC},i}^6 \overset{\epsilon \to h\nu}{\longrightarrow} R_\infty^6\left(\epsilon\right) = \frac{3\,(\hbar c)^4}{4\pi} \frac{\sigma_{\mathrm{PI}}^{(\mathrm{B})}\left(\epsilon\right)}{\epsilon^4}, \tag{13}$$

   which is thereby independent of the particular species capturing the free electron species and even the capturing channel i.

The overall characteristic distance of the ICEC process exhibits a maximum, defining an optimal starting energy for the experimental observation of ICEC in any system. Moreover, it has been shown to be bound by the same quantities R_{max} in magnitude and $R_\infty(\epsilon)$ in its large-energy convergent behaviour as each individual channel i described in equations (12) and (13). These quantities are solely dependent on the assisting partner molecule and provide an easily accessible first estimate for feasibility of ICEC in any potential future experimental setup. Hence, the ICEC radius depends on the intrinsic properties of the individual units and provides a new and intuitive design tool.

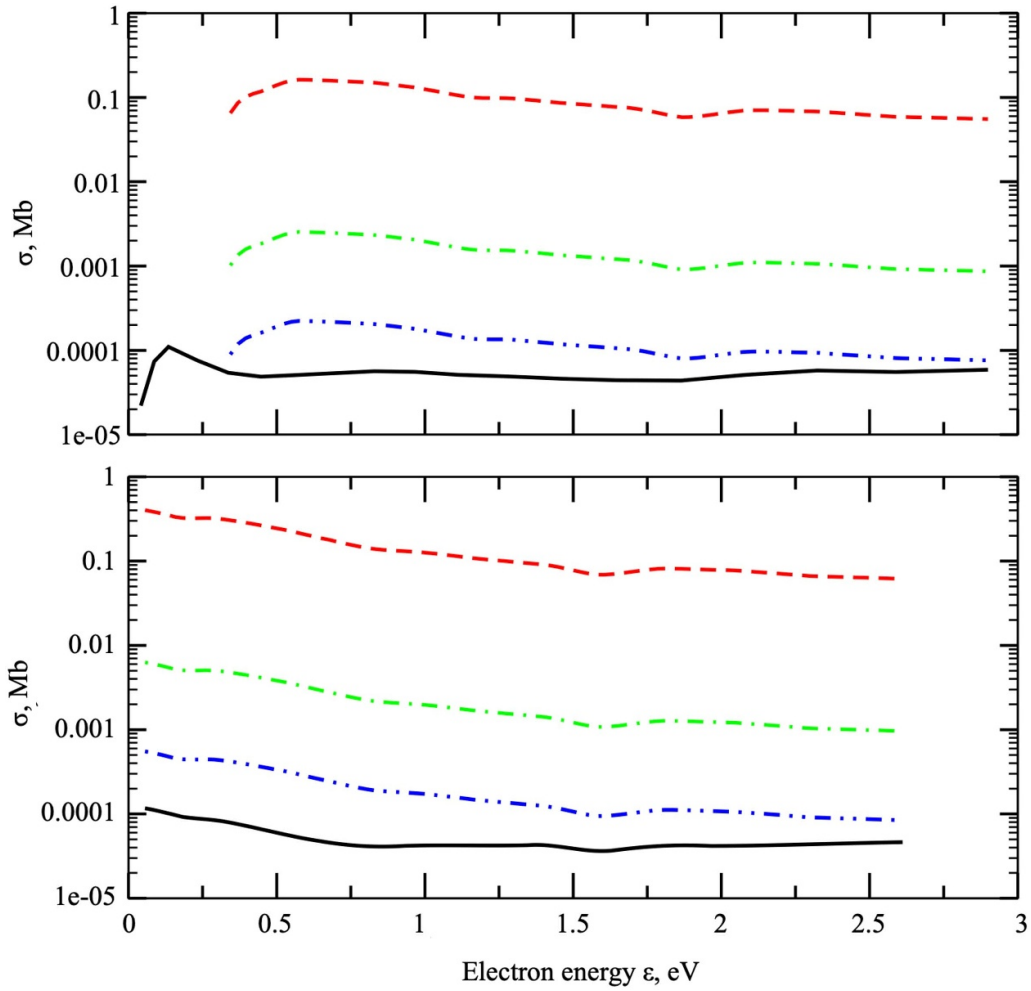

Figure 4. ICEC cross sections for a capture into the ground states for upper panel: $Br + Cl^-$ and lower panel: $Cl + Br^-$ at different interatomic distances. The solid black line shows the photo-recombination cross section of the electron capturing unit, while the coloured lines account for different internuclear distance, where blue corresponds to 3 nm, green to 2 nm and red to 1 nm, respectively. Reproduced from [25].

2.2. Systems

Real systems exhibit at least a subset of the above-mentioned processes. Hence, the cross sections can never be accounted for by a single effect. In the following, we introduce the systems investigated within the asymptotic approximation and highlight the effects of channel openings, distance dependence, energy of the incident electron, and ionization cross sections of unit B.

2.2.1. $Br + Cl^-$ and $Cl + Br^-$. One of the first ICEC processes to be investigated was the electron capture on a halogen atom accompanied by the electron emission from a different halide [20, 25]. When considering the net reaction only, that is ignoring the electron on both sides of the chemical equation,

$$e + \mathrm{X} + \mathrm{Y}^- \rightarrow \mathrm{X}^- + \mathrm{Y} + e', \tag{14}$$

one may assume that an electron is transferred from the halide to the halogen atom. While this charge exchange process can occur at very small interatomic distances, where the components' wavefunction significantly overlap, at larger distances an ICEC process is a much more plausible explanation. As a consequence, the electron can here be seen as a catalyst for the net electron transfer reaction.

In this halogen-halide example the importance of channel openings based on the energy balance can be illustrated in a disentangled way. For reasonably slow incident electrons, only a capture to the ion's ground state is energetically accessible. While the ICEC process is available for any electron energy in the $Cl + Br^- \rightarrow Cl^- + Br$ case (see lower panel in figure 4), the reverse process requires a minimum kinetic energy of the incident electron of at least 0.288 eV [25]. This becomes noticeable by a later onset of the ICEC cross section in the upper panel of figure 4.

In addition to this, figure 4 shows that the ICEC process (coloured lines) is more efficient than the corresponding photo-recombination process (solid black line) for as much as 3 nm. This can be attributed to both the low transferred energy between the units as well as the high photo-ionization cross section of the bromide and chloride anions.

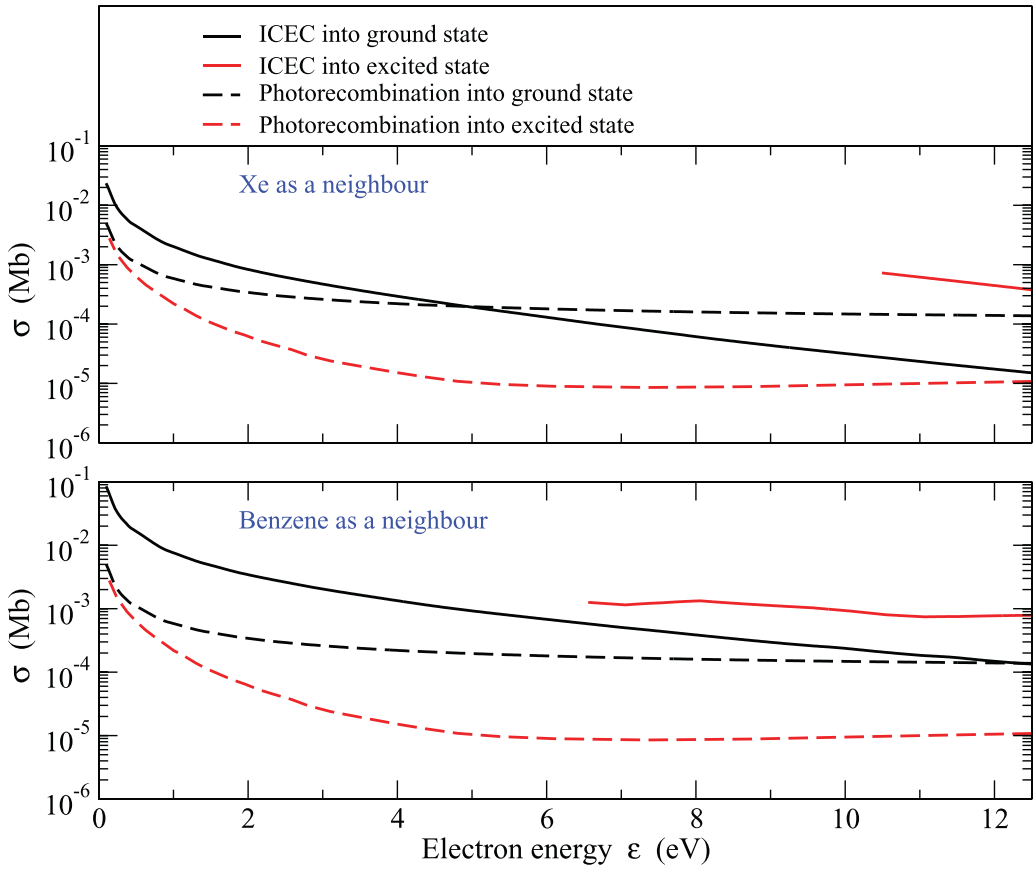

Figure 5. ICEC cross sections for an electron capture of different kinetic energies ε by a neon-cation with either a xenon atom or a benzene molecule as partner. The ICEC cross sections are given as solid lines with an ICEC process for an electron capture into the ground state is shown in black and an ICEC process initiated by an electron capture into an excited state is shown in red. The respective photo-recombination cross sections are given as dashed lines as comparison. The simulations were carried out for an interparticle distance of 1 nm. Reprinted figure with permission from [20], Copyright (2010) by the American Physical Society.

2.2.2. Ne^+ with Xe or benzene. When the electron is captured by the neon cation and ICEC proceeds with either a xenon atom or a benzene molecule in the vicinity a plethora of different processes is possible. Consequently, this constitutes an ideal showcase scenario despite the low absolute ICEC cross sections caused by the rather high energy transferred between the two units, particularly in the case of a capture into the ground state.

With a ground state electron affinity of 21.565 eV and ionization potentials of SIP(Xe) = 12.13 eV and SIP(Bz) = 9.45 eV, the direct ICEC channel is open for all kinetic energies of the incident electron. This can be seen in figure 5 as solid black line. The ICEC cross section decreases for higher incident electron energies, because the transferred energy increases and lowers the cross section according to equation (6). The detailed behaviour of the ICEC cross sections is caused by the energy dependence of the neighbours photo-ionization cross section.

Alternatively, the neon cation can also capture the electron into the excited 3*p*-Rydberg state with an electron affinity of 2.943 eV. The direct ICEC channel for a capture into an excited state is therefore closed for slow incident electrons. However, it opens at higher kinetic energies of the incident electron and is shown as solid red lines in figure 5. Because the single ionization potential of benzene is lower than of xenon, the ICEC channel for a capture into the excited state opens at lower incident electron energies.

The corresponding photo-recombination cross sections of the neon cation are also displayed in figure 5 as dashed lines. Please note that the photo-recombination cross sections significantly decrease upon capture of the incident electron into an excited state. Therefore, the corresponding cross sections are usually neglected. For the ICEC process, on the other hand, an electron capture into an excited state reduces the energy being transferred between the two units. Therefore, according to equations (6) and (7), the corresponding cross section for an electron capture into an excited state is larger than for an electron capture into the ground state.

As already mentioned, the neon cation in combination with a xenon atom or a benzene molecule can undergo different types of ICEC. As shown in [20], a dielectronic resonance-enhanced ICEC process is initiated by an electron capture into one of the Rydberg *p*-orbitals under excitation of another electron from the 2*s* orbital to the 2*p*-orbital. Here, the ICEC cross section was shown to be governed by the efficiency of the RICD process following the electron capture into the resonance state.

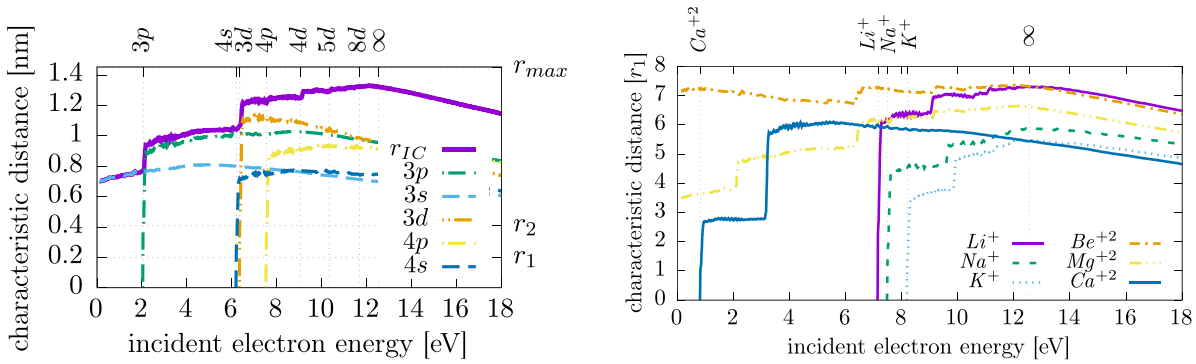

Figure 6. The ICEC radius for water-assisted capture as function of energy, (left) across different capture channels for the established theory test case of $[e^- + Mg^{2+}]$ near H_2O, and (right) across different biorelevant alkaline and alkaline-earth cations in water assistance in terms of the characteristic length of their respective hydration shell radii r_1. Reprinted from [36], with the permission of AIP Publishing.

2.2.3. Alkali or alkaline earth metal ion with a water molecule. A yet rare example of a testbench system for different levels of theoretical approaches toward ICEC is the bio-relevant magnesium dication Mg^{2+} in proximity of an assisting water molecule which has been originally proposed for ICEC [25] and discussed for its potential cascades of related intermolecular energy transfer processes [38, 39], before it has been reinterpreted and expanded across the other alkaline and alkaline-earth cations in terms of their respective ICEC radius [36]. It is thus an interesting system to test alternative numerical approaches beyond the asymptotic approximation (cf section 3.3 for a discussion on *R*-matrix investigations of a microhydrated proton as technical precursor system, and section 5.3 for a discussion on its perspectives towards microhydrated alkaline and alkaline-earth metal cations) [36].

Within the original communication of ICEC, assisted electron capture into the ground state 3*s* orbital was suggested for Mg^{2+} in proximity of a water molecule at selected fixed distances [25, 40]. Despite ignoring any capture channels beyond the ground state, it demonstrates that ICEC is efficient and dominant over environment-independent photorecombination of Mg^{2+} for fixed examples of intermolecular distance between Mg^{2+} and assisting water molecule [25, 40]. This provided the initial postulate for ICEC as an efficient capture process in general, however it was not yet addressed at that time how to compare different systems and different interatomic distances consistently, nor how to relate Mg^{2+} with water to typical distances like first or second hydration shell radius (r_1, r_2), or how to evaluate the intermolecular reach of ICEC, as well as the role of excited orbitals as capture channels.

Motivated by its biological relevance as hydrated mineral, and by the question on secondary slow-electron processes in biological systems in consequence of initial radiation damage [28], Mg^{2+} with water has been reinvestigated since then on its potential for non-local energy transfer cascades through ICD and electron transfer mediated decay (ETMD) [38, 41]. It remained unclear then what the net effect of multistate capture would contribute through ICEC: the capturing state for electron capture cannot be controlled externally; instead all electronic states that meet the energy threshold arising from equation (3) are contributing to the overall ICEC cross section which provides a stark contrast to the conceptual investigation of a selected distinct two-site excited state decaying through ICD and related decay processes [36].

With the very recent interpretation of an intermolecular-distance-independent scaled amplification factor in form of the ICEC radius (cf equation (9)) [36], it was thus possible to investigate the contribution of all open capture channels to the dominant range of ICEC in water assistance with respect to the environment-independent photorecombination of Mg^{2+} with a free electron. Figure 6 (left panel) shows the respective contributions of leading individual capture channels to the overall ICEC radius as function of incident electron energy. It has thereby been shown that the primary contribution to ICEC can not intuitively be attributed to a ground state capture.

Moreover, the representation of ICEC in terms of its ICEC radius provided a clear indication for consistent step over from ICEC to ETMD at the energetic conceptual limit of 0 eV as incident free energy threshold. ICEC is exothermic for Mg^{2+} near H_2O, that means the ICEC pathway is already open at the 0 eV free energy edge. Conceptually this extends down to 2.32 eV below the electronic continuum threshold [36, 42, 43]. The ICEC radius and the energetic difference according to equation (3) therefore indicate that Mg^{2+} would be able to steal an energetically highly bound electron by assistance of the water molecule as conceptual extension of ICEC from low energetic free electrons to bound Rydberg electrons through ETMD. On the other hand, it was found that the large energy behaviour of each capture channel's contribution to the ICEC radius becomes independent of the particular channel. Instead, it shows a clear signature of the assisting water molecule and can be therefore easily predictable theoretically and recognisable by potential future experiments.

In the picture of the ICEC radius, it was thus possible to compare the interatomic range of ICEC to a typical distance for the system of Mg^{2+} with an assisting water molecule: the first hydration shell radius, r_1, that indicates a natural equilibrium distance between the cation and the next neighbour water molecule in a solution. It was found here that even with the restriction of a pure dimer interaction, still neglecting the multiple available contributing partner molecules in a condensed

matter environment, ICEC dominates over photorecombination to up to 6.5 multiples of r_1 [36].

Furthermore, the biological importance of Mg^{2+} in interaction with water imposes the question on ICEC efficiency with respect of other alkaline and alkaline-earth cations that act as essential nutrient minerals and often show a complex antagonistic relationship with respect to biological absorption in the presence of each other in solution [44]. In this context, it appears more relevant to accommodate for the differences in typical equilibrium distances of the respective mineral in water. It was thus compared across the board for alkaline monocations and alkaline-earth dications from Li^+ to K^+, and from Be^{2+} to Ca^{2+} in terms of their respective hydration shell radius r_1, as presented in figure 6 (right panel). It has thereby been shown that ICEC is endothermic for the alkaline monocations and for the calcium dication but has a significant dominance over photorecombination at typical intermolecular distances from its energetic threshold onward. At its respective optimal incident energy every individual investigated cation reaches dominance over photorecombination, as indicated by its respective ICEC radius, for intermolecular distances between 5.5 multiples of its respective typical r_1 (in case of K^+) and 7.35 multiples of r_1 (in the case of Be^{2+}) [36]. Moreover, its been made apparent that across the board, the higher energy behaviour of the ICEC radius is consistently independent on the particular electron captor species, and instead purely determined by the assisting water molecule according to equation (13).

3. ICEC in atomic and molecular dimers

So far, for large donor-acceptor distances within the virtual photon approximation, we have neglected the orbital overlap between the donor and acceptor species. However, in nature, it is likely that the two subsystems approach one another enough so that the absence of orbital overlap is not a valid approximation anymore. Hence, to go beyond the asymptotic limit, one has to employ a method that explicitly includes the possibility of orbital overlap.

3.1. The R-matrix approach

The R-matrix technique allows to go beyond the asymptotic derivation very efficiently. In particular, in this approach the electron correlation, which is the driving force of ICEC, can be properly accounted for. The R-matrix method has been widely and successfully employed to describe scattering between molecules, atoms and electrons as well as reactions in nuclear, atomic, and molecular physics. It has been only recently that its usefulness in the context of ICEC has been established [37, 45, 46].

The R-matrix theory divides a physical problem into an inner and an outer region separated by a sphere of radius a centred at the centre of mass of the system. The inner region contains the multi-particle description of the full system composed of $N+1$ electrons. In the outer one only a free particle (here the incoming or the outgoing ICEC electron) is treated and its interaction with the N remaining particles (electrons) is described in terms of a multipole expansion of the N-electronic density.

The wave function ansatz of the inner-region wavefunction is in terms of a configuration interaction (CI) expansion:

$$\Psi(\mathbf{x}_1,\mathbf{x}_2,\ldots,\mathbf{x}_{\mathbf{N}+1}) = A\sum_{ij}\alpha_{ijk}\phi_i(\mathbf{x}_1,\mathbf{x}_2,\ldots,\mathbf{x}_{\mathbf{N}})\,u_{ij}(\mathbf{x}_{\mathbf{N}+1}) + \sum_i \beta_{ik}\chi_i(\mathbf{x}_1,\mathbf{x}_2,\ldots,\mathbf{x}_{\mathbf{N}+1})\ . \quad (15)$$

ϕ_i is the many-particle CI wavefunction of the so-called target state i, u_{ij} are orbitals introduced to represent the scattered electrons, both the incoming and the ICEC electron. The operator A ensures the antisymmetry of the wavefunction. In the second term, χ_i are the so-called L^2 configurations that allow correlation and polarization effects. The R-matrix at the boundary a between the inner and outer regions can be obtained from the solutions of the time-independent Schrödinger equation using the above ansatz (i.e. from the diagonalization of the Hamiltonian CI-matrix). The R-matrix is then numerically propagated from $r=a$ to ∞, where the scattering amplitudes ($f_{0j}(\Omega)$) are extracted, from which cross sections and resonance widths can then be obtained. A detailed description of the R-matrix method can be found in these reviews [47, 48].

The R-matrix method has been employed to study ICEC in the mixed rare-gas clusters $Ne^+@He_n$ as well as to investigate the ICEC electron attachment to a proton in the neighbourhood of a water molecule [37, 45, 46]. We summarize in what follows the main findings.

3.2. ICEC in mixed rare-gas clusters

The first application of the R-matrix approach in ICEC was published in 2018 and dealt with the Ne^+-He dimers as well as larger clusters, i.e. $Ne^+@He_{20}$. The aim of this work was threefold: (1) to investigate the effect of the orbital overlaps on the ICEC cross sections, (2) to determine the validity of the virtual photon approximation and (3) to study ICEC in large-sized clusters that can be probed experimentally.

The main findings are that when the donor and the acceptor species are close enough, the ICEC process can be up to two orders of magnitude larger than predicted by the virtual photon approximation formula and up to four to five orders of magnitude larger than radiative recombination cross sections. To illustrate this, in figure 7 we display the ICEC cross sections for two incoming electron energies as a function of the $NeHe^+$ distance. It is clearly shown that the virtual photon approximation underestimates the cross sections for distances below 3.5 Å whereas for larger distances it becomes valid. In [45], it was also shown that an additive pairwise approximation (i.e. the ICEC cross sections in the presence of several acceptor neighbours are the sum of the cross sections for each donor-acceptor pair) is valid in these mixed rare-gas clusters. To demonstrate the validity of this additive pairwise approximation the authors compared, for the same Ne–He distances the ICEC cross sections, computed with the R-matrix

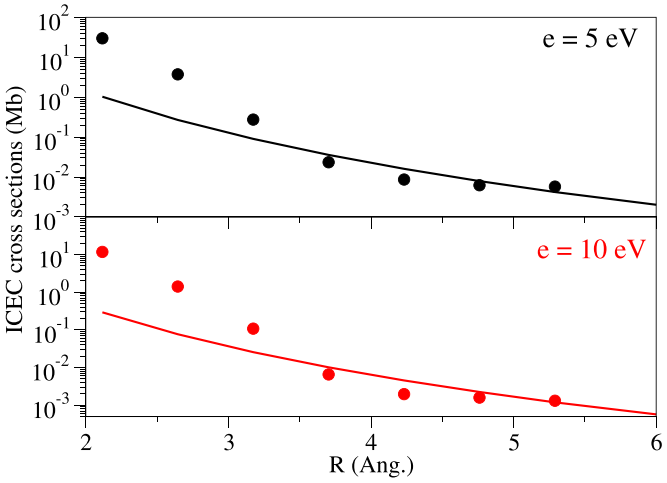

Figure 7. ICEC cross sections as a function of the NeHe distance for two incoming electron energies: 5 eV (top panel) and 10 eV (bottom panel). The lines report the cross sections from the virtual photon approximation. The dots show the ICEC cross sections obtained from the *R*-matrix calculations (see [45] for details). Reprinted figure with permission from [45], Copyright (2018) by the American Physical Society.

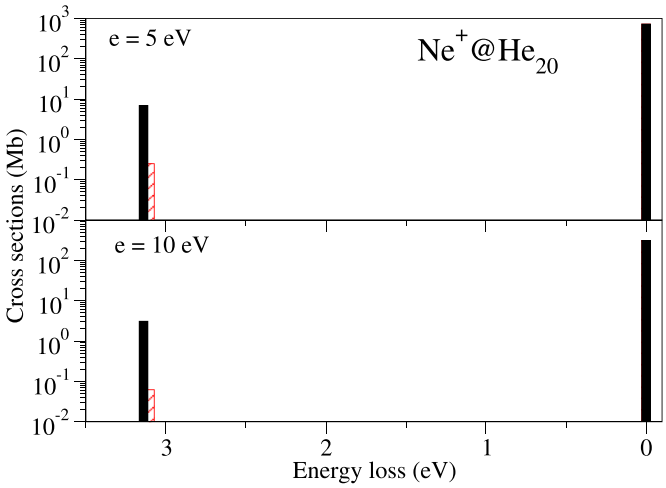

Figure 8. Energy loss (or ICEC) spectra (in Mb) for Ne^+ embedded in He_{20} clusters for two incoming electron energies: 5 eV (top panel) and 10 eV (bottom panel). Full black bars report the *ab initio* *R*-matrix calculations. Red dashed bars show results obtained employing the asymptotic formula (see [45] for details). Reprinted figure with permission from [45], Copyright (2018) by the American Physical Society.

method, for Ne^+-He with that of Ne^+-He_2 where the ion is centred between the two helium atoms. They found that the ratio between the corresponding cross sections ($\sigma_{He_2}/\sigma_{He}$) is approximately two.

Using the additive pairwise approximation, the ICEC cross sections in larger systems can easily be calculated. The energy loss (or ICEC) spectra for Ne^+ embedded in He_{20} clusters for two incoming electron energies are shown in figure 8. It should be highlighted that the wavefunction for Ne^+@He_{20} employed to model ICEC was taken from a variational quantum Monte Carlo calculation (see [45] for more details). Energy loss spectra are generally employed in electron-molecule collision experiments. The energy loss peak corresponding to ICEC is sufficiently high to be measured: they are equal to about 7 and 3 Mb for $e = 5$ and 10 eV, respectively. In both cases, they are higher by nearly two orders of magnitude than predicted by the asymptotic formula, and four to five orders of magnitude higher than the radiative recombination cross sections. It should also be noted that the ICEC cross sections are only two orders of magnitude smaller than the elastic ones, illustrating quantitatively the ICEC efficiency. These results should pave the way to the first experimental observations of ICEC (see section 5).

3.3. *ICEC in the proton-water dimer*

The second study on ICEC using the *R*-matrix approach focused on the electron recombination with a proton in the presence of a water molecule. This represents a simple model for microhydrated cations which are relevant in radiation biological damage [37, 46]. The authors focused on proton-water distances between 3 and 8 Å. These values correspond to the second and third hydration shells in condensed phases, respectively. While this range is relevant to biological and biochemical systems, it should be noted that as protons are extremely reactive they would also strongly interact with the first shell of water molecules. This, of course, may influence the ICEC process between the proton and a second water molecule in a higher shell. The *R*-matrix results reported in [37, 46] are therefore only a very first step in modelling and understanding ICEC in biological and biochemical systems.

Unexpectedly, the *ab initio* ICEC cross sections for a proton-water systems exhibit some structures. These features were shown to be Fano profiles coming from interference between two pathways leading to the same final states, the direct ICEC pathway and the one via a series of metastable electronic states where the incoming electron is temporarily bound to the donor-acceptor system. Several of those metastable states, contributing to the Fano interferences, were identified: H(1*s*)-$H_2O(^3A_1, 1b_2 \rightarrow 2b_2)$, H(1*s*)-$H_2O(^1A_1, 1b_2 \rightarrow$ Rydberg) but also H^+-H_2O^- and H^{-*}-H_2O^+.

Figure 9 shows the ICEC cross sections (for $e + H^+$-$H_2O(\tilde{X}) \rightarrow$ H(1s)-$H_2O^{+(*)} + e'$) as a function of the energy of the incoming electron, the cross sections were multiplied by R^6 in order to compare the different distances on the same scale. The *R*-matrix ICEC cross sections exhibit these Fano profiles that are superimposed to the smooth cross sections computed within the virtual photon approximation (see [37, 46] for further details). Due to these Fano interferences, the ICEC cross sections can be substantially enhanced or suppressed. This opens the way to control of electron recombination processes.

To gain further insights into the interferences between the quantum paths, the authors analysed the Fano profiles by fitting them with the following equation (see [49])

$$\sigma \propto \frac{\left(\tilde{E}+q\right)^2}{1+\tilde{E}^2}. \tag{16}$$

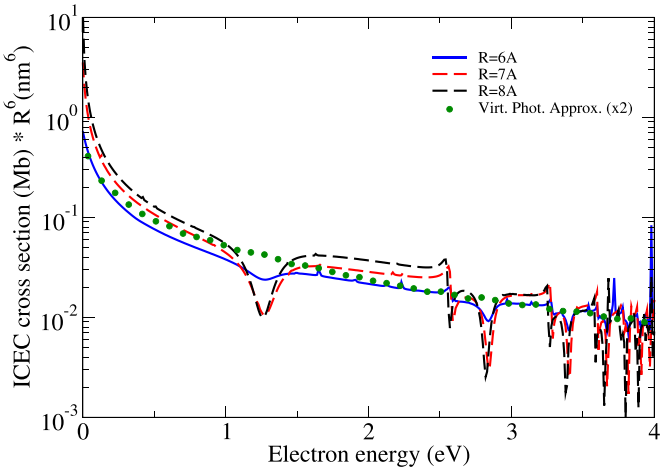

Figure 9. Total ICEC cross sections multiplied by R^6 (for $e + H^+$-$H_2O(\tilde{X}) \rightarrow H(1s)$-$H_2O^{+(*)} + e'$) as a function of the energy of the incoming electron. The results computed with the *R*-matrix approach for different distances between the proton and the oxygen atom of the water molecule are represented by lines . These results are compared with those of the virtual photon approximation (green dots). The cross sections obtained from the virtual photon approximation were multiplied by 2 for visualization (see [37, 46] for details). Reprinted figure with permission from [37], Copyright (2021) by the American Physical Society. Reprinted figure with permission from [46], Copyright (2021) by the American Physical Society.

In the above equation, q is the asymmetry parameter and $\tilde{E}$ is called the reduced energy

$$\tilde{E} = 2\left(\epsilon - E_i\right)/\Gamma_i \tag{17}$$

where E_i and Γ_i are the position and width of the resonance state, respectively. In Fano theory, the asymmetry parameter q is defined as a ratio of the transition probabilities to the resonance state and to the continuum. When $|q|$ is of the order of 1, the transitions through the continuum and resonance state are of the same strength, resulting in the asymmetric Fano profile. In the limit where $|q|$ is very large, the transition to the continuum is very weak and the transition through the resonance state largely dominates. Conversely, in the case where $q = 0$ the cross section is described by a symmetrical dip around the position of the resonance state. In [37, 46], the authors found $q = 0.03$ for the lowest profile and between 0.6 and 1.0 for the higher ones, showing that around the incoming electron energy of 1.3 eV the ICEC process is mostly a direct process. It should be noted, however, that although there is nearly no transition through the resonance state, the presence of the latter leads to a substantial decrease of the ICEC cross sections in the respective electron energy range. At higher electron energies the paths through the resonance states play an equally important role as the direct one.

In [46], which is a follow-up paper of [37], the authors investigated the partial ICEC cross sections in the proton-water system. This study showed that the Fano interferences favour ionization of the water molecule in the $(3a_1^{-1}, {}^2A_1)$ state compared to direct photoionization. Ionization of water is an important process for radiation damage studies. The results reported in [46] demonstrated that the environment around water can significantly change the ionization of these molecules and should therefore be taken into account in future investigations.

The works summarized above have demonstrated that the *R*-matrix method is a powerful tool to investigate ICEC in atomic and molecular clusters. It is also clear that much more has to be learned in ICEC. These works represent therefore only the very first step in the *ab initio* study of ICEC.

4. ICEC in quantum dots

As seen, the concept of ICEC is rather simple. It requires nothing beyond two spatially separated subsystems with one (or few) bound electronic levels fulfilling the ICEC energy condition. Therefore, building on the existing examples of atoms and molecules, the next logical step is to use 'artificial atoms' or QDs. These are nanostructures that share optical and/or other properties with naturally occurring atoms [50, 51]. A similar generalization as we show here for ICEC was possible for the related ICD process [52, 53].

In this section we explain the standard models used to compute electronic properties in few-electron QDs (section 4.1). Given the small number of active electrons, the QD models allow an execution of explicit electron-dynamics calculations of ICEC. This has in the past been done with the multiconfiguration time-dependent Hartree method (MCTDH, cf section 4.2). Investigations so far targeted ICEC involving only two electrons, one in each QD, where direct ICEC has been observed (section 4.3). Moreover, a novel resonance-enhanced pathway has been discovered and analyzed in connection with the ICD (sections 4.4 and 4.5).

4.1. Modelling paired semiconductor quantum dots

QDs are semiconducting, solid-state materials shrunk to nanometer size that were first experimentally obtained by Chang *et al* [54] and by Reed *et al* [55]. Numerous nanoscale materials have been developed since then [10, 56]. The very common GaAs semiconductors (doped with Al or In) are our focus here. Other common III–V semiconductor QDs are made of InP [57, 58]. Significant examples of II–VI semiconductors are CdS [11], ZnO, or ZnS [58] and even silicon-based materials [59] have been designed and created relying on the advanced silicon manufacturing technology. Finally, it should be highlighted that carbon-based structures are promising candidates that aim to provide ecologically responsible and sustainable technological applications [60, 61].

The electronic structure is determined by the material. Given its effective mass m^* and the dielectric constant ε_r of a typical semiconductor ($\varepsilon_r \approx 10\,\varepsilon_0$ and $m^* \approx 0.05\,m_e$), the effective Bohr radius $a^* \approx a_0 \frac{\varepsilon_r}{\varepsilon_0}\frac{m_e}{m^*}$ of an artificial hydrogen atom, i.e. a single-electron spherical QD, is about 10 nm (see chapter 5 of [62] for an introduction to effective-mass theory).

Effectively, QDs are structures whose conduction band states are occupied only by a few active electrons. Occupation with conduction band electrons results from optical excitation,

charging via electromagnetic fields [57, 63], or doping [64]. The QDs can thus be described by a simple model potential that confines electrons in a potential (e.g. square well, Gaussian, etc).

The simplicity of these systems readily enables QD design via geometry and size. Another means of control and design these nanostructures is by employing more than one QD [57, 65–67]. In this case, the simplest system of interacting QDs is a pair, which can be categorized in two groups as a function of interaction strength. Coupled, or double, QDs (DQD) are molecule-like constructions, where the orbitals resemble molecular orbitals. Conversely, paired QDs (PQDs) are more distant and, as a consequence, they exhibit atom-like, separate orbitals in each QD; electron exchange can be excluded here. Since ICEC is clearly identified for well-separated sites, this section focuses on PQDs.

In figure 10(a) the ICEC process in general Gaussian binding potentials is visualized as it applies to PQDs. An electron impinging from the left is captured by the left potential into its L_0 level while the right potential, originally binding an electron on the R_0 level, is ionized. The energy conservation

$$E_T = E_{R_0} + \varepsilon = E_{L_0} + \varepsilon', \tag{18}$$

applies [20] (see also equation (3)) .

In equation (18) the energies of the incoming (i) and the outgoing (f) electrons are defined through their associated momenta $p_{i,f}$ according to $\varepsilon = p_i^2/2$ and $\varepsilon' = p_f^2/2$ with the mass being unity in our effective atomic units. $\Delta E = E_{R0} - E_{L0}$ is here the transferred excess energy. Depending on the relative energy of the two levels involved, L_0 and R_0, the emitted electron can have a higher ($\Delta E > 0$) or lower ($\Delta E < 0$) momentum than the initial one, $\varepsilon' = \varepsilon + \Delta E$.

Many experimental devices used in transport studies embed the QD in a nanowire, a nanostructure with quasi-dimensional geometry [57, 68–71]. Hence we propose to study the two-electron effective-mass model for a PQD in a nanowire. The Hamiltonian is explicitly given by

$$\hat{H}(\mathbf{r}_1, \mathbf{r}_2) = \hat{h}(\mathbf{r}_1) + \hat{h}(\mathbf{r}_2) + \frac{1}{\varepsilon_r |\mathbf{r}_1 - \mathbf{r}_2|}, \tag{19}$$

where ε_r in the Coulomb interaction term is the relative dielectric permittivity and

$$\hat{h}(\mathbf{r}_i) = -\frac{1}{2m^*}\nabla_i^2 + V_c(x_i, y_i) + V_l(z_i), \tag{20}$$

is a one-electron Hamiltonian in which

$$V_c(x_i, y_i) = \frac{1}{2} m^* \omega^2 (x_i + y_i)^2 \text{ and} \tag{21}$$

$$V_l(z_i) = -V_L e^{-b_L(z_i + R/2)^2} - V_R e^{-b_R(z_i - R/2)^2}, \tag{22}$$

are the transversal confined and the longitudinal open potentials, respectively. R is the distance between the centres of the QDs, $b_{L,R}$ are parameters quantifying the sizes of the left (L) and right (R) QDs, and $V_{L,R}$ represent their energetic depths.

Since our main goal is to provide a simple model in which ICEC is clearly spotted, we proposed to solve the above general nanowire model in the strong lateral confinement regime. This allows to derive a set of effective one-dimensional working equations. In fact, if V_L and V_R are both much smaller than $\hbar\omega$, one can prove that the wave function ansatz,

$$\Psi(\mathbf{r}_1, \mathbf{r}_2) = \psi(z_1, z_2)\, \phi_0(x_1, y_1)\, \phi_0(x_2, y_2), \tag{23}$$

reproduces very well the 3D model results [72], provided that ϕ_0 is the 2D harmonic oscillator ground state. Using (23), a two-particle one-dimensional Hamiltonian can be found for $\psi(z_1, z_2)$ (an example of what is called envelope function [73]), where the Coulomb term is replaced by the effective interaction,

$$V_{eff}(z_{12}) = \sqrt{\frac{\pi}{2}} \frac{1}{l} e^{\zeta^2} (1 - erf(\zeta)), \tag{24}$$

which depends on $\zeta = |z_1 - z_2|/\sqrt{2}l$ and the electron–electron distance scaled by the confinement size $l = \sqrt{\langle\phi_0|x^2|\phi_0\rangle}$. This term has no divergence at $\zeta = 0$ (for finite l) and scales as $\frac{1}{|z_1 - z_2|}$ for long electron distances.

4.2. MCTDH for electron dynamics

The numerical demonstration of the inter-QD Coulombic electron capture could, in principle, be done by means of electronic-structure theory through consideration of the initial and final states only, which can be many if continuum is concerned. However, an explicit electron dynamics description, achieved through the explicit solution of the time-dependent Schrödinger equation, can be numerically advantageous regarding the description of the electronic continuum, despite the potentially higher computational cost arising from the time propagation. Furthermore, they provide complementary physical insight into the process.

Several explicit electron dynamics methods exist [74], but, whatever the choice to describe ICEC, the method has to be flexible to properly describe different kinds of electronic states. Indeed, the ICEC process involves free electrons (captured and emitted) as well as bound electrons in the initially and finally occupied QD orbitals. In our case, MCTDH is the method of choice owing to its versatility in describing such quickly changing character of the electrons; for more details we refer the reader to the first works on the method and the book [75–77]. One of the main reasons behind this is the use of a time-dependent basis (with an underlying time-independent discrete-variable representation) in combination with compact (low-rank) sum-of-products *ansätze* for the representation of all quantities involved in the MCTDH dynamics such as operators or, in particular, the wavefunction. It should be highlighted that the latter can be readily antisymmetrized.

In the specific example of a QD in a wire with quasi one-dimensional confinement, the initially scattering electron is defined as a one-dimensional Gaussian wavepacket,

$$f_{WP_i}(z) = \frac{1}{\sqrt{\Delta z}(2\pi)^{1/4}} e^{-1/4(z - z_0/\Delta z)^2} e^{ip_i(z - z_0)}, \tag{25}$$

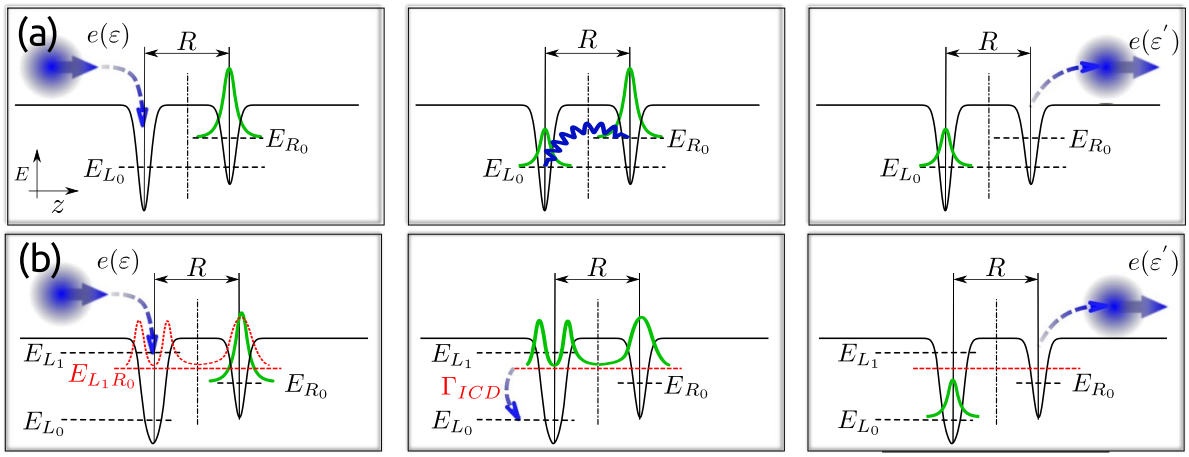

Figure 10. Schematic representation of two-electron ICEC processes in QDs. (a) In direct ICEC, the left QD captures a free electron (blue left) with kinetic energy ε into the level L_0. Simultaneously, the excess energy is transmitted and the electron from the R_0 level of the neighbouring QD is emitted with energy ε'. (b) In the resonance-enhanced ICEC process the capture of the electron $e(\varepsilon)$ from the left occurs into the resonance state L_1R_0, which is delocalized over both QDs and decays via ICD, releasing likewise an electron of energy ε'.

with an initial spatial width Δz approaching on the z axis from z_0 with the initial momentum p_i. Note that the Gaussian is spatially broad when compared to the bound R_0 function. So in order to avoid the overlap of both single-electron initial functions, the Gaussian has to be placed relatively far from the QD pair, i.e. the absolute value of z_0 needs to be large, leading likewise to a significantly larger grid as known from the previous ICD MCTDH investigations [52]. It should be emphasized that such large one-dimensional grids lead to computational and numerical issues when dealing with high-dimensional calculations. Hence, the utilization of tensor decomposition methods is imperative [78], whether in a grid-based [79] or grid-free [80] form.

With respect to the electronic wavefunction, the two single-electron wavefunctions, the Gaussian and the R_0 eigenfunction, combine antisymmetrically into the triplet state

$$\Psi(z,z',t=0) = 1/\sqrt{2}\,(f_{WP_i}(z)\,\phi_{R_0}(z') - \phi_{R_0}(z) f_{WP_i}(z'))\,. \tag{26}$$

The propagation can most illustratively be followed through the visualization of the time evolution of the electronic density $\rho(z,t) = \int |\Psi(z,z',t)|^2 \mathrm{d}z'$, from which momenta of the initial and final wavepackets can be qualitatively deduced. Furthermore, this quantity directly provides the relative importance of the different channels as well as the relative timings.

A quantitative analysis is available through the measurement of the electron flux into complex absorbing potentials (CAPs) [81]. The CAPs themselves, $\hat{W}_{\mp} = -i\eta(z \pm z_{\mathrm{cap}})^n \Theta(z \pm z_{\mathrm{cap}})$, prevent electrons from artificial reflection at both ends of the grid. $\Theta(z)$ is the Heaviside function and the intensive strength parameter η is chosen as to minimize both reflection and transmission through the CAP, as this maximizes the absorption of density. To measure the ICEC electron only (not any non-reactive incoming electron), we use the projected flux [82],

$$g_{L_0}(\tau) = 2\int_0^\infty \langle \Psi(t)\,|P_{L_0}^{(1)} \hat{W}_+^{(2)} P_{L_0}^{(1)}|\,\Psi(t+\tau)\rangle \mathrm{d}t. \tag{27}$$

This quantity records only the absorption of one electron in positive z direction (W_+), while the other is bound to the L_0 state. One can normalize the projected flux in relation to the energy spread, $|\Delta E_{WP_i}(E_T)|^2$, of the initial wavepacket giving with that a reaction probability (RP) of [82],

$$RP = 100 \times \frac{2\mathrm{Re}\int_0^\infty g_{L_0}(\tau)\, e^{-iE_T\tau}\,\mathrm{d}\tau}{\pi |\Delta E_{WP_i}(E_T)|^2}. \tag{28}$$

It should highlighted that this quantity is wavepacket independent.

4.3. Direct ICEC

The first case in which ICEC was observed with MCTDH was the scenario shown in figure 10(a) [72, 83]. As an illustrative example, we consider two GaAs QDs of size ≈10 nm separated by a distance of $R \approx 100$ nm and with $\Delta E = 1.55$ meV. The size of impinging wavepacket is $\Delta z_{WP_i} \approx 100$ nm and it has an energy of $\varepsilon_{WP_i} = 1.542$ meV (see [84] for more details).

The visualization of the electron density as function of z and time (see figure 11) clearly shows how the incoming wavepacket approaches the R_0-bound electron represented by a thin density around $z = R/2$, the latter remains qualitatively unchanged over time. The scattering electron impinges from beyond $z = -980$ nm with a much broader spatial width distribution. Within 15–18 ps in time the ever widening wavepacket reaches the bound electron and Coulomb repulsion causes it to be scattered back to a large extent. However, a small fraction of the electron density leaves the PQD system to the right with a momentum of $p_f = 0.0485$ meV·ps nm^{-1}, at the instant of the interaction. This change in momentum perfectly matches the expectation for ICEC in a case where $\Delta E > 0$; note that under different energy settings a decelerating ICEC process is likewise possible [85]. This constitutes the first manifestation of ICEC in an electron dynamics calculation [72, 83].

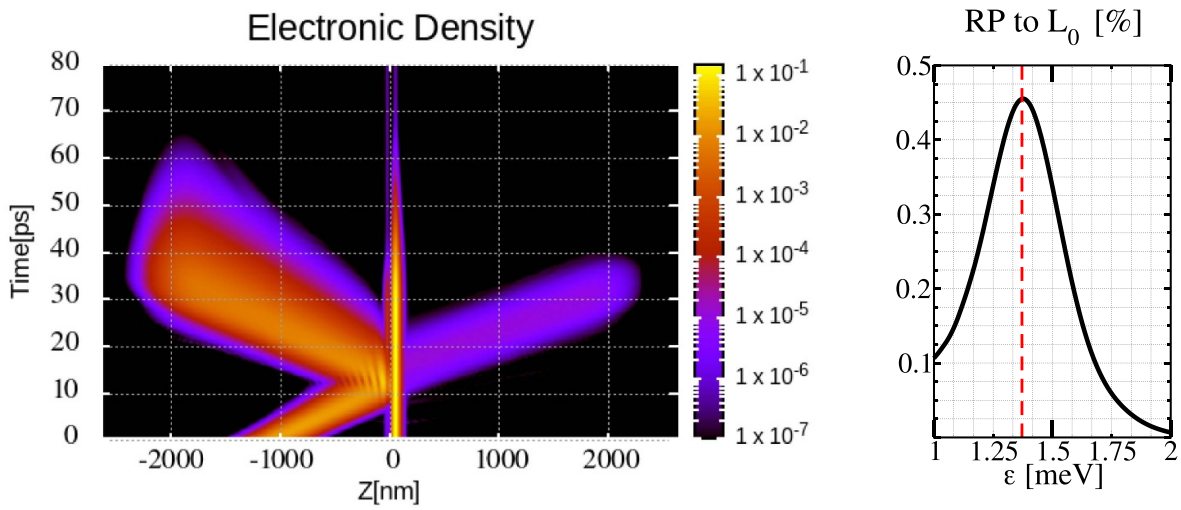

Figure 11. Time-dependent electronic density for an ICEC process in a PQD and its corresponding reaction probability. Note that the incoming electronic density from the left has a different slope than the emitted ICEC electron to the right, indicating the inelastic momentum transfer derived from equation (18). The reaction probability shows a Gaussian shaped energy dependence with a peak value of ≈0.5%. Reproduced from [72]. © IOP Publishing Ltd. All rights reserved.

As a second analysis, the RP for ICEC was calculated according to equation (28). It is a function of the energy of the incoming electron with a near-Gaussian shape that peaks at one certain $\varepsilon_i^{(\mathrm{peak})}$. With a 0.5% value, the maximal RP is very low but nonetheless proof that an intricate process such as ICEC in QDs is possible. The RP distribution as a function of ε implies two things. First, incoming electrons of different velocities can undergo ICEC, each at its own probability. Second, there is an energy selectivity for ICEC. A comparison of system parameters reveals that $\varepsilon_i^{(\mathrm{peak})}$ locates at $\varepsilon_i^{(\mathrm{peak})} \approx E_{L_0} - 2E_{R_0} = 1.37$ meV which in turn maps back to the total energy during ICEC, $E_T^{(\mathrm{peak})} = -\Delta E$.

Another analysis to confirm the inelastic scattering quality of the direct ICEC process is via the Gaussian shape of the energy-resolved projected flux representation [86]. Figure 12(a) shows predominantly the setting (b_L parameter different from the default introduced above) of a direct ICEC process. Here the expected Gaussian peak 'G' appears at the total energy, i.e. at $E_T = -2.2$ meV.

4.4. Resonance-enhanced ICEC in quantum dots

With the notion of ICEC enhancement in mind (cf section 2) [20, 25], which is presumably caused by additional resonance channels, we also sought such resonance-enhanced pathways in QDs with the tool of reaction probability as well as the projected energy-resolved flux.

From previous research, we know that an L_1R_0 state can decay via ICD into a final state with an electron in the L_0 level and the other in the ionization continuum, as depicted in panel (b) of figure 10 [52]. L_1 is the upper of two states in the left QD, for which the explicit energies $E_{L_0} = -5.22$ meV and $E_{L_1} = -0.57$ meV were used. They locate below and above, respectively, the sole level R_0 of the right QD. They satisfy both the ICD energy condition $E_{L1} - E_{L0} \geqslant |E_{R0}| = 2.92$ meV and the ICEC energy condition $E_T = E_{R_0} + \varepsilon = E_{L_0} + \varepsilon'$ with $\Delta E > 0$. To keep the investigation simple, a direct capture into the L_1 level is energetically forbidden by design.

By simple inspection of the density evolution in figure 13 we can observe how the impinging electron approaches the PQD and is progressively captured into the final L_0 level. This process includes the instantaneous backscattering along a persistent slope as well as direct ICEC with a reduced slope according to the velocity of the ICEC electron. In addition, over a time interval about 2.5 times as long as the completed backscattering, electron density is leaving the paired QD system predominantly to the left side. It fades exponentially and is a clear indication that the ICD resonance has temporarily been populated. A second indication for this is that at the position $-R/2$ where the left dot is located, a double-peaked density, signature of the excited L_1 level, appears at the moment of scattering.

The reaction probability energy distribution in this example is much more narrow and peaks at a lower $\varepsilon_i^{(\mathrm{peak})} = 0.59$ meV, to which it is difficult to assign a shape. This means that the energy selectivity is significantly enhanced for ICEC. But in that case it happens at a significantly higher probability of 22%. Comparison with the energy parameters of the system shows that such strong enhancement is obtained when $E_T \approx E_{L_1R_0} = 0.61$ meV $+ E_{R_0}$ (solid green line in figure 13). Again the time-energy uncertainty allows one to obtain a resonance decay time of $\tau_{\mathrm{ICEC}}^{\mathrm{GaAs}} = 14.26$ ps, which is ten times slower than direct ICEC. Hence, the resonance enhanced ICEC process is highly probable and more selective in energy than direct ICEC. However, it is slower than direct ICEC.

The RP alone and likewise the energy-dependent projected flux of the given case are not fully clear on the interplay among the direct and the resonance-enhanced ICEC channel. Comparison among different settings (here different b_L)

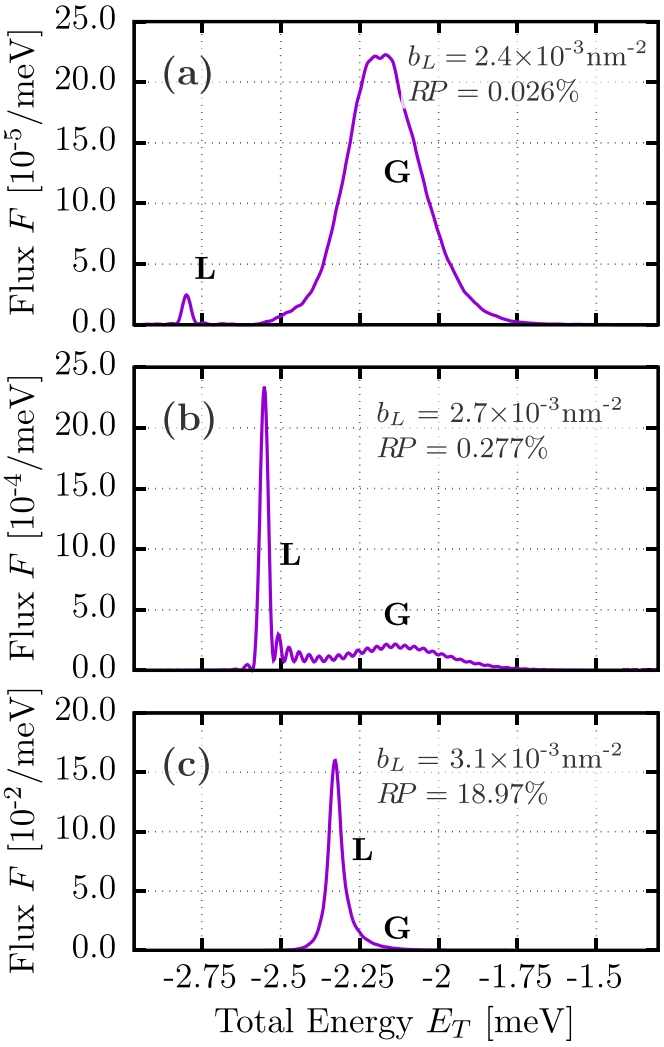

Figure 12. All panels show the flux as function of the total energy E_T for different b_L giving different RP's. 'G' and 'L' denote a Gaussian and Lorentzian flux and refer to the direct ICEC and the resonance-enhanced ICEC process, respectively.

returns figures of still rather low RP, with two distinct peaks (figures 12(a) and (b)). One is the Gaussian peak of direct ICEC at constant energy position, the second one indicated with 'L'. From panels (a) to (c) the energy $|E_{L_1}|$ decreases and the 'L' peak energy follows this change from $E_T = -2.798$ meV over -2.549 meV to -2.324 meV while the peak intensity more and more dominates over that of the Gaussian and enhances at the same time the overall flux. The peak is rationalized to be a Lorentzian, the standard distribution after the decay of a resonance state [87]. Including the ICD rate Γ_{ICD} it reads

$$F_{L_0}^{\mathrm{res}}(E) \propto \frac{\Gamma_{\mathrm{ICD}}^2}{4\left(E - E_{L_1R_0}\right)^2 + \Gamma_{\mathrm{ICD}}^2}. \tag{29}$$

Despite the maximized energy-resolved flux at the overlay of the Gaussian and the Lorentzian, in our investigations this was not necessarily the case with the largest ICEC probability. And indeed there is a second effect determining the wavepacket-independent quantity RP: it is the definition of the initial wavepacket. It enters the RP (equation (28)) through the denominator that incorporates division by $|\Delta E_{WP_i}(E_T)|^2$, the energy widths. This means that all the contributions of the flux that are exactly in the range of initial wave packet give a reduced RP even when the two ICEC peaks perfectly overlay [86]. This signifies that ICEC from a wavepacket is not only sensitive to confinement sizes, but likewise to the incoming wavepacket. In contrast, if the large Lorentzian contribution is located at the tail of ΔE_{WP_i}, the RP experiences an enhancement even though the electronic structure is unfortunate in the sense that the direct and the resonance-enhanced ICEC channels do not overlay inside the width of the wavepacket.

4.5. Interplay of direct and resonance-enhanced ICEC

If different QD energy levels are to be compared, then it is advisable to use an energetically wide wave packet. This was done in a study where the quantum-size effect [56, 88, 89] was explored to determine the overall largest possible RP in a PQD. To this end a scan over about 8000 QD geometries (b_L, V_L, R) was undertaken, which resulted in an empirical understanding of the interdependence of the ICEC probability on single-electron level energy relations useful for the *a priori* decision on whether a certain atomic, molecular, or nano-sized system is capable of ICEC or not [72].

Several conditions were set up and probed in the given parameter space. Of the trivial ones, one is the boundary conditions $E_{L_1} = 0$, which determines whether there is a second energy level L_1 in the left dot that could be available to resonance-enhanced ICEC or not. Following directly on that is the condition that L_1R_0 is a resonance (and no bound) state given through $E_{L_1R_0} = E_{R_0}$. The existence of the resonance gives rise to another three conditions that determine the position of the largest RP, each at least on a distinct area of the total (b_L, V_L) parameter plane. One of these conditions is $E_{L_1R_0} = E_{L_0} - E_{R_0}$, which reflects the coincidence of the direct (accelerating) and the resonance-enhanced ICEC channel. As in this scan, the direct (slowing) ICEC via occupation of the L_1 level is not excluded, also the coincidence of that channel and resonance-enhanced ICEC leads to high rates following the energy condition $E_{L_1R_0} = E_{R_0} - E_{L_1}$. Last, but not least, also the two direct channels can occur simultaneously even without the resonance pathway involved. Then $E_{L_1} - E_{R_0} = E_{R_0} - E_{L_0}$ must hold.

The efficiency can be explored by scanning the maximum RP (colour bar in figure 14) for each configuration on the (b_L, V_L) planes for different R's. The above conditions can be confirmed from areas of zero RP and a branching line of maximal RP (close to a Y shape). The largest RP exceeds 50% for $R = 88.14$ nm as shown in figure 14. It occurs when the conjunction of three conditions is synergistic and enables the stronger increase of the ICEC probability. The three conditions for the largest RP can be evaluated *a priori* from single-electron energies alone [72]. This prediction is applicable to all possible systems beyond models and can apply to atom and molecule pairs as well.

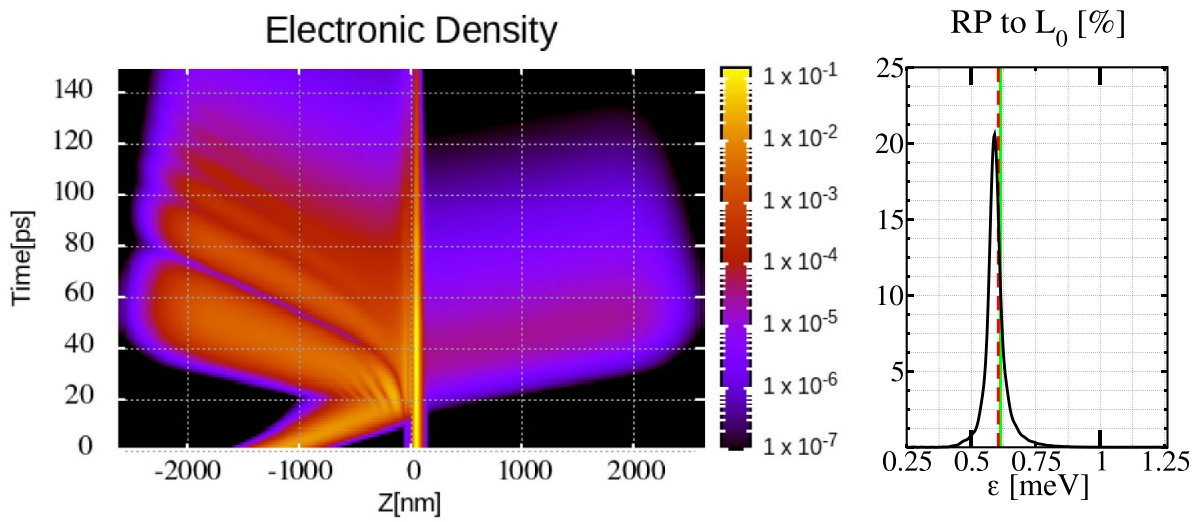

Figure 13. Time dependent electronic density for a resonance-enhanced ICEC process in a PQD and its corresponding reaction probability. Note that the reaction probability shows a Lorentzian shaped energy dependence in this case and has peak value of 20%, this is 40 times larger than direct ICEC. The time-energy uncertainty allows to obtain a resonance decay time of $\tau_{\mathrm{ICEC}}^{\mathrm{GaAs}} = 14.26$ ps, which is ten times slower as direct ICEC. Hence, an interesting trade off between a slower, selective and highly probable process (resonance enhanced) and a faster (direct) process is present. Note that the range in this figure is the same as in figure 11 (1 meV). The green solid line indicates the $E_{L_1R_0}$ resonance energy at $\varepsilon_i = 0.61$ meV. Reproduced from [72]. © IOP Publishing Ltd. All rights reserved.

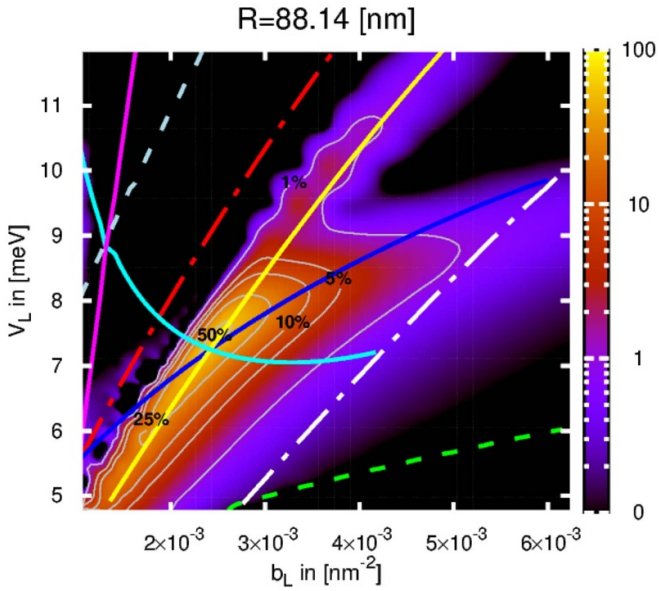

Figure 14. Maximum of the RP as a function of the geometric parameters b_L (inverse of left QD size) and V_L (left QD depth). The contour grey lines indicate the RP level. The coloured lines corresponds to some energy condition that is fulfilled along it. The best geometry is at the crossing of the cyan line ($E_{L_1R_0} = E_{L_0} - E_{R_0}$, resonance enhanced ICEC to L_0) and the yellow line ($E_{L_1R_0} = E_{R_0} - E_{L_1}$ resonance-enhanced ICEC to L_1). Reproduced from [85]. © IOP Publishing Ltd. All rights reserved.

4.6. Conclusion and outlook on QD ICEC research

Likewise to atomic and molecular systems, electron capture itself is an emerging topic in QD research. And much like what is found for atoms/molecules, capture happens by redistribution of the excess energy onto other degrees of freedom. While the energy transfer to the phonons of the system is most prominent [90–95], energy transfer to the electrons can lead to different follow-up settings: Excited states that store multiple excitons [96] or induce Auger relaxations [97], as well as the ICEC process.

The studies on ICEC in QDs were, however, not only driven by the fundamental curiosity on the generality of the process, on its enhancement factors, and on a fundamental understanding of its drivers [52, 72, 83, 85, 86]. One significant aspect is its anticipated application in modern miniature electronic devices. With miniaturization such devices are beyond the regime of classical physics and governed by quantum-mechanical effects [98]. Among the four basic elements of all nano-electronic devices [99]—resistor, capacitor, (light-emitting) diode and transistor—ICEC may be instrumentalized in a transisting one. Certain electrons are blocked while others can enter the device via capture depending on their velocity. If successfully captured, the electronic structure of the device determines if the ICEC electron proceeding through the circuit at the other side is faster or slower than the captured ones. Its speed can be tuned by setting the relative energies in the QD pair, e.g. electrostatically. In the context of miniaturization, the QDs in nanowires [57, 68–71] analysed in the presented works are optimal candidate structures to achieve the recent goal of further miniaturization in nano-electronics, where systems on chips operating different logic functionalities are expected to be as small as 2 nm in 2025 [100].

5. Perspectives

5.1. Experimental demonstration of ICEC

As a first remark, it should be emphasized that there is no experimental observation yet of ICEC processes. Measuring

ICEC is hence an obvious and crucial need. At the time of writing this review, several international groups are working on the development of the techniques necessary for such measurements. One of the simplest systems to demonstrate ICEC might be $Ne^+@He_n$ (see section 3.2). Indeed, such systems are simple enough to be prepared and, as shown above, ICEC would provide a clear signature in the electron energy loss spectrum. We hope that this topical review will help them in their efforts and will encourage more groups to tackle such difficult but essential tasks.

5.2. ICEC in ultracold atoms

Beyond rare-gas clusters $Ne^+@He_n$ (see section 3.2) as a possibility of future experimental observation of ICEC, it appears of interest to investigate electron dynamics of ICEC in the domain of ultracold-atom physics. This domain has seen a considerable growth but has not been addressed in the context of non-local continuum energy transfer processes. Of particular interest could be the investigation of a heteronuclear ultracold atom–ion pair [101], where an analogous experiment appears within reach [102–105].

A frozen-core description is therefore proposed as initial venture into atomic assisted electron-capture dynamics in which an ionic Ba^{2+} core could be modelled with an incident electron e of kinetic energy ε in a local subsystem, that is in interaction with an assisting distant subsystem of an ionic Rb^+ core with a reactive outer valence electron initially bound in the rubidium $5s$ level to form a ground state rubidium atom, Rb [101]. The assisting rubidium subsystem can then mitigate electron capture on the barium site through ICEC by emitting its modelled outer valence electron with kinetic energy ε':

$$\left[e\left(\varepsilon\right)+\mathrm{Ba}^{2+}\right]+\mathrm{Rb}\longrightarrow\mathrm{Ba}^{+}+\left[\mathrm{Rb}^{+}+e\left(\varepsilon'\right)\right]. \qquad (30)$$

Promising indications of electron capture stemming from interatomic energy transfer are already seen in this quantum-dynamical exploratory work at experimentally relevant macroscopic interatomic distances [106]. This present research project ventures into the first highly-correlated electron dynamics of two free electrons in a three-dimensional continuum. It aims at exploring a complementary research direction within current initiatives in the scientific community of electron dynamics in the context of inter-Coulombic processes. As such, it is expected to yield results that will shed light on findings from other research endeavours.

5.3. ICEC in microhydrated cations

Radiation from the Sun, radioactive substances, or x-rays can cause damage in living organisms. Indeed, it has been recently found that the damage due to radiation can spread exponentially through the human body by a cascade of decay processes of chemical compounds which release numerous slow electrons [38, 39]. Decay processes related to radiation damage include Auger decay, interatomic Coulombic decay, superexchange ICD, and ETMD, which have attracted considerable attention over the last decade [107].

Free electrons are genotoxic agents since they can break up chemical bonds by attaching themselves to neighbouring atoms. This is called DEA [26–28]. As shown above, ICEC leads to a strong enhancement of electron attachment. ICEC might thus be a general process that controls damage of living cells under ionizing irradiation. It is therefore highly relevant to investigate ICEC in biological model systems and thus reveal its potential impact on radiation damage.

Overall, up to 60% of the adult human body consists of water and even the bones contain 31% water [108]. Furthermore, metals [109] are comprised by about 2% in total. In their ionic form they regulate fluid flow into and out of body cells, blood pressure, muscle contractions and nerve signals and heart activity. More importantly, they are the key ingredient to complex chemical structures called coordination compounds, in which a central metal atom is surrounded by groups of non-metal molecular structures, called ligands. An important example for such complexes is haemoglobin, which contains a central iron atom. It gives blood its red colour and carries the vital oxygen through our body to the organs.

Metal cations are biologically abundant and they are expected to be strongly ICEC-active owing to their large electron affinity. As discussed in section 2.2.3, it was indeed shown using the virtual photon approximation that ICEC is very efficient in micro-hydrated cations [36]. To gain more insights, one can/should however go beyond the virtual photon approximation and investigate *ab initio* systems containing a metal cation and few water molecules. The *R*-matrix method, as discussed above in section 3, is the primary choice for these studies and has proven successful in initial proof-of-concept explorations for microhydrated proton (see in particular section 3.3) [37, 46].

5.4. Impact of the nuclear dynamics on ICEC

As shown above, the theoretical approaches employed to describe ICEC range from analytical models to *ab-initio* electronic structure and dynamical calculations. A common assumption in these approaches is that nuclei remain fixed during ICEC. However, based on observations on the related ICD process [110, 111], nuclear dynamics should play an important role changing the efficiency and/or influencing the final state of the system. Investigating the impact of the nuclear dynamics on ICEC is therefore crucial. However, this requires a significant methodological and numerical development. At time of writing this review, the authors are implementing such project which is supported by a German and French collaboration through an ANR-DFG program.

Two kinds of nuclear degrees of freedom should be investigated: in the first, one can focus on the impact of the nuclear motion along the axis between the ICEC donor and acceptor species. As shown above, the ICEC cross sections vary substantially along this distance and a large effect of the nuclear dynamics is therefore expected. A second kind of nuclear motion that can impact ICEC is the intramolecular vibrational motion of the donor and/or acceptor species. For these modes, it is difficult to anticipate the effects on ICEC processes.

Data availability statement

No new data were created or analysed in this study.

Acknowledgments

We thank the ANR-DFG for financial support of the QD4ICEC project. The respective DFG Grants are BA 3770/5-1 and FA 1989/1-1; the ANR Grants are ANR-22-CE92-0071-01 and ANR-22-CE92-0071-02. E F gratefully acknowledges financial support from the research and service facility LISA$^+$ of the University of Tübingen. F M P gratefully acknowledges partial financial support of CONICET(PIP-KE311220210100787CO), SECYT-UNC (Res. 233/2020) and ANPCYT-FONCyT, PICT-2018 No. 3431. A B is grateful for the funding received through the Freigeist fellowship (89525) from Volkswagen Foundation. Financial support for the work of A M has been gratefully received from the Research Foundation—Flanders (FWO) within the Junior Postdoctoral Fellowship Mandate 1232922N, and from the Fulbright Schuman-Program Award issued by The Commission for Educational Exchange between the United States, Belgium and Luxembourg. This recognition does not imply that the Government of the United States or any agency representing it has endorsed the conclusions or approved the contents of this publication.

ORCID iDs

Annika Bande https://orcid.org/0000-0003-3827-9169
Elke Fasshauer https://orcid.org/0000-0001-8187-6052
Axel Molle https://orcid.org/0000-0002-4383-4377
Daniel Peláez https://orcid.org/0000-0003-3924-7804
Federico M Pont https://orcid.org/0000-0003-3161-6206
Nicolas Sisourat https://orcid.org/0000-0002-8567-5263

References

[1] Tucker W H 1975 *Radiation Processes in Astrophysics* (MIT University Press)
[2] Carelli F, Grassi T and Gianturco F A 2013 *Astron. Astrophys.* **549** A103
[3] Summers H P and Dickson W J 1992 *Applications of Recombination* (Plenum)
[4] Hörndl M, Yoshida S, Wolf A, Gwinner G, Seliger M and Burgdörfer J 2006 *Phys. Rev.* A **74** 052712
[5] Evans D H 2008 *Chem. Rev.* **108** 2113
[6] Mason N J 2008 *Int. J. Mass Spectrom.* **277** 31
[7] Ho W 1994 *Surf. Sci.* **299–300** 996
[8] Garrett B C *et al* 2005 *Chem. Rev.* **105** 355
[9] Kumar A, Becker D, Adhikary A and Sevilla M D 2019 *Int. J. Mol. Sci.* **20** 3998
[10] García de Arquer F P, Talapin D V, Klimov V I, Arakawa Y, Bayer M and Sargent E H 2021 *Science* **373** eaaz8541
[11] Carey G H, Abdelhady A L, Ning Z, Thon S M, Bakr O M and Sargent E H 2015 *Chem. Rev.* **115** 12732
[12] Chutjian A, Garscadden A and Wadehra J 1996 *Phys. Rep.* **264** 393
[13] Ingólfsson O, Weik F and Illenberger E 1996 *Int. J. Mass Spectrom. Ion Process.* **155** 1
[14] Pshenichnyuk S A, Asfandiarov N L, Vorob'ev A S and Matejčík Š 2022 *Phys.-Usp.* **65** 163
[15] Fasshauer E 2023 Schematic figures for ICEC review (available at: https://doi.org/10.6084/m9.figshare.23496827)
[16] Jacob A, Müller C and Voitkiv A B 2019 *Phys. Rev.* A **100** 012706
[17] Eckey A, Jacob A, Voitkiv A B and Müller C 2018 *Phys. Rev.* A **98** 012710
[18] Voitkiv A B and Najjari B 2010 *Phys. Rev.* A **82** 052708
[19] Müller C, Voitkiv A B, López-Urrutia J R C and Harman Z 2010 *Phys. Rev. Lett.* **104** 233202
[20] Gokhberg K and Cederbaum L S 2010 *Phys. Rev.* A **82** 052707
[21] Jacob A, Zhang S F, Müller C, Ma X and Voitkiv A B 2020 *Phys. Rev. Res.* **2** 013105
[22] Remme S, Voitkiv A B and Müller C 2023 *J. Phys. B: At. Mol. Opt. Phys.* **56** 095202
[23] Photorecombination is a process in which a free electron is attached to a system and the excess energy is released through emission of a photon. It is the inverse of photoionization/photodetachment
[24] Massey H S W and Bates D R 1942 *Rep. Prog. Phys.* **9** 42
[25] Gokhberg K and Cederbaum L S 2009 *J. Phys. B: At. Mol. Opt. Phys.* **42** 4
[26] Boudaïffa B, Cloutier P, Hunting D, Huels M A and Sanche L 2000 *Science* **287** 1658
[27] Alizadeh E, Orlando T M and Sanche L 2015 *Annu. Rev. Phys. Chem.* **66** 379
[28] Sanche L 2016 *Radiat. Phys. Chem.* **128** 36
[29] Taylor J P 2006 *Scattering Theory* (Dover)
[30] Schroeder D V and Peskin M E 1995 *An Introduction to Quantum Field Theory* (Westview Press)
[31] Averbukh V, Müller I B and Cederbaum L S 2004 *Phys. Rev. Lett.* **93** 263002
[32] Gokhberg K, Kopelke S, Kryzhevoi N V, Kolorenč P and Cederbaum L S 2010 *Phys. Rev.* A **81** 12
[33] Fasshauer E, Pernpointner M and Gokhberg K 2013 *J. Chem. Phys.* **138** 014305
[34] Fowler R H and Milne E A 1925 *Proc. Natl Acad. Sci.* **11** 400
[35] In an autoionization process, the system releases its excess energy by ejecting an electron from the same unit that is excited
[36] Molle A, Zatsarinny O, Jagau T, Dubois A and Sisourat N 2023 *J. Chem. Phys.* **158** 134306
[37] Molle A, Dubois A, Gorfinkiel J D, Cederbaum L S and Sisourat N 2021 *Phys. Rev.* A **103** 012808
[38] Stumpf V, Gokhberg K and Cederbaum L S 2016 *Nat. Chem.* **8** 237
[39] Gokhberg K, Kuleff A I and Cederbaum L S 2021 *Electronic Decay Cascades in Chemical Environment* (Elsevier) p 163
[40] Ivanov V K, West J B, Gribakin G F and Gribakina A A 1994 *Z. Phys.* D **29** 109
[41] ETMD is a non-local decay process, as ICD. In ETMD, an electron is transferred from one unit of the whole system to another unit and a second electron is ejected. There are several variants of ETMD depending on which unit ejects the second electron. These variants are not discussed here
[42] Heays A N, Bosman A D and van Dishoeck E F 2017 *Astron. Astrophys.* **602** A105
[43] Mendoza C 1996 *Phys. Scr.* **T65** 198
[44] Behar J 1975 *Am. J. Physiol.* **229** 1590
[45] Sisourat N, Miteva T, Gorfinkiel J D, Gokhberg K and Cederbaum L S 2018 *Phys. Rev.* A **98** 020701(R)
[46] Molle A, Dubois A, Gorfinkiel J D, Cederbaum L S and Sisourat N 2021 *Phys. Rev.* A **104** 022818
[47] Tennyson J 2010 *Phys. Rep.* **491** 29

[48] Mašín Z, Benda J, Gorfinkiel J D, Harvey A G and Tennyson J 2020 *Comput. Phys. Commun.* **249** 107092
[49] Fano U 1961 *Phys. Rev.* **124** 1866
[50] Schedelbeck G, Wegschneider W, Bichler M and Abstreiter G 1997 *Science* **278** 1792
[51] Zrenner A 2000 *J. Chem. Phys.* **112** 7790
[52] Bande A, Gokhberg K and Cederbaum L S 2011 *J. Chem. Phys.* **135** 144112
[53] Cherkes I and Moiseyev N 2011 *Phys. Rev.* B **83** 113303
[54] Chang L L, Esaki L and Tsu R 1974 *Appl. Phys. Lett.* **24** 593
[55] Reed M A, Randall J N, Aggarwal R J, Matyi R J, Moore T M and Wetsel A E 1988 *Phys. Rev. Lett.* **60** 535
[56] Alivisatos A P 1996 *Science* **271** 933
[57] Salfi J, Roddaro S, Ercolani D, Sorba L, Savelyev I, Blumin M, Ruda H E and Beltram F 2010 *Semicond. Sci. Technol.* **25** 024007
[58] Eren G O *et al* 2021 *ACS Appl. Mater. Interfaces* **13** 32022–30
[59] Lim W H, Huebl H, Willems van Beveren L H, Rubanov S, Spizzirri P G, Angus S J, Clark R G and Dzurak A S 2009 *Appl. Phys. Lett.* **94** 173502
[60] Yan X, Li B and Li L-S 2013 *Acc. Chem. Res.* **46** 2254
[61] Biercuk M J, Garaj S, Mason N, Chow J M and Marcus C M 2005 *Nano Lett.* **5** 1267
[62] Dresselhaus M, Dresselhaus G, Cronin S and Gomes Souza Filho A 2018 *Solid State Properties* (*Graduate Texts in Physics*) (Springer)
[63] Mi X, Benito M, Putz S, Zajac D M, Taylor J M, Burkard G and Petta J R 2018 *Nature* **555** 599
[64] Mocatta D, Cohen G, Schattner J, Millo O, Rabani E and Banin U 2011 *Science* **332** 77
[65] Collini E *et al* 2020 *J. Phys. Chem.* C **124** 16222
[66] Nilsson M, Chen I-J, Lehmann S, Maulerova V, Dick K A and Thelander C 2017 *Nano Lett.* **17** 7847
[67] Mittag C *et al* 2021 *PRX Quantum* **2** 010321
[68] Leturcq R, Stampfer C, Inderbitzin K, Durrer L, Hierold C, Mariani E, Schultz M G, von Oppen F and Ensslin K 2009 *Nat. Phys.* **5** 327
[69] Roddaro S, Pescaglini A, Ercolani D, Sorba L and Beltram F 2011 *Nano Lett.* **11** 1695
[70] Nadj-Perge S, Pribiag V S, van den Berg J W G, Zuo K, Plissard S R, Bakkers E P A M, Frolov S M and Kouwenhoven L P 2012 *Phys. Rev. Lett.* **108** 166801
[71] van der Wiel W G, De Franceschi S, Elzerman J M, Fujisawa T, Tarucha S and Kouwenhoven L P 2002 *Rev. Mod. Phys.* **75** 1
[72] Pont F M, Bande A and Cederbaum L S 2016 *J. Phys.: Condens. Matter* **28** 075301
[73] Bastard G 1991 *Wave Mechanics Applied to Semiconductor Heterostructures* (*Monographs of Physics (Les Editions de Physique)* vol 1) (Wiley)
[74] Bande A 2022 *Chemical Modelling* (Royal Society of Chemistry) pp 91–152
[75] Meyer H-D, Gatti F and Worth G A 2009 *Multidimensional Quantum Dynamics: MCTDH Theory and Applications* (Wiley)
[76] Meyer H-D, Manthe U and Cederbaum L 1990 *Chem. Phys. Lett.* **165** 73
[77] Manthe U, Meyer H-D and Cederbaum L S 1992 *J. Chem. Phys.* **97** 3199
[78] Haller A, Peláez D and Bande A 2019 *J. Phys. Chem.* C **123** 14754
[79] Peláez D and Meyer H-D 2013 *J. Comput. Phys.* **138** 014108
[80] Panadés-Barrueta R L and Peláez D 2020 *J. Comput. Phys.* **153** 234110
[81] Riss U V and Meyer H-D 1996 *J. Chem. Phys.* **105** 1409
[82] Beck M H, Jäckle A, Worth G A and Meyer H D 2000 *Phys. Rep.* **324** 1
[83] Pont F M, Bande A and Cederbaum L S 2013 *Phys. Rev.* B **88** 241304(R)
[84] Settings of the QDs according to Eq.(22) for the direct ICEC simulation: QDs separated by a distance of $R = 97.94$ nm. The lower-energy level L_0 with $E_{L_0} = -4.47$ meV in the left QD and the R_0 level with $E_{R_0} = -2.92$ meV in the right QD. Impinging wavepacket defined via its momentum $p_i = 0.0343$ meV ps nm^{-1} as well as its spatial width, $\Delta z_{WP_i} = 97.94$ nm. This corresponds to an energy of $\varepsilon_{WP_i} = 1.542$ meV and an energy width of $\Delta E_{WP_i} = 0.391$ meV. The rest of the parameters are $V_R = 7.11$ meV, $1/\sqrt{b_R} = 9.79$ nm, $V_L = 9.48$ meV and $1/\sqrt{b_L} = 9.79$ nm
[85] Pont F M, Molle A, Berikaa E R, Bubeck S and Bande A 2020 *J. Phys.: Condens. Matter* **32** 065302
[86] Molle A, Berikaa E R, Pont F M and Bande A 2019 *J. Chem. Phys.* **150** 224105
[87] Rosas-Ortiz O, Fernández-García N and Cruz y Cruz S 2008 *AIP Conf. Proc.* **1077** 31
[88] Rossetti R, Ellison J L, Gibson J M and Brus L E 1984 *J. Chem. Phys.* **80** 4464
[89] Alivisatos A P 1996 *J. Phys. Chem.* **100** 13226
[90] Seebeck J, Neilsen T R, Gartner P and Jahnke F 2005 *Phys. Rev.* B **71** 125327
[91] Glanemann M, Axt V M and Kuhn T 2005 *Phys. Rev.* B **72** 045354
[92] Prasankumar R P, Upadhya P C and Taylor A J 2009 *Phys. Status Solidi* b **246** 1973
[93] Porte H P, Uhd Jepsen P, Daghestani N, Rafailov E U and Turchinovich D 2009 *Appl. Phys. Lett.* **94** 262104
[94] Zibik E A *et al* 2009 *Nat. Mater.* **8** 803
[95] Jiang F, Jin J, Wang S and Yan Y J 2012 *Phys. Rev.* B **85** 245427
[96] Nozik A J, Beard M C, Luther J M, Law M, Ellingson R J and Johnson J C 2010 *Chem. Rev.* **110** 6873
[97] Narvaez G, Bester G and Zunger A 2006 *Phys. Rev.* B **74** 075403
[98] Vogel E 2007 *Nat. Nanotechnol.* **2** 25
[99] Datta S 2018 *Nat. Electron.* **1** 500
[100] The International Roadmap Committee (IRC) 2021 *International Roadmap for Devices and Systems™: More Moore* (IEEE) p 7
[101] Molle A 2019 Electron dynamics of interatomic coulombic electron capture in artificial and real atoms *PhD Thesis* Freie Universität Berlin (http://dx.doi.org/10.17169/refubium-25683)
[102] Wolf J, Deiß M, Krükow A, Tiemann E, Ruzic B P, Wang Y, D'Incao J P, Julienne P S and Denschlag J H 2017 *Science* **358** 921
[103] Sikorsky T, Meir Z, Ben-shlomi R, Akerman N and Ozeri R 2018 *Nat. Commun.* **9** 920
[104] Bahrami A, Müller M, Drechsler M, Joger J, Gerritsma R and Schmidt-Kaler F 2019 *Phys. Status Solidi* b **256** 1800647
[105] Franssen J G H, de Raadt T C H, van Ninhuijs M A W and Luiten O J 2019 *Phys. Rev. Accel. Beams* **22** 023401
[106] Molle A, Drennhaus J P, Noel V, Kolev N, Vendrell O and Bande A 2023 Time-resolved rubidium-assisted electron capture by barium (II) cation (arXiv:2306.09580 [physics.atom-ph])
[107] ICD/ICEC Publication List (available at: www.pci.uni-heidelberg.de/tc/usr/icd/ICD.refbase.html)
[108] Mitchell H H, Hamilton T S, Steggerda F R and Bean H W 1945 *J. Biol. Chem.* **158** 625
[109] Forbes R M, Mitchell H H and Cooper A R 1956 *J. Biol. Chem.* **223** 969
[110] Scheit S, Meyer H-D and Cederbaum L S 2005 The interatomic Coulombic decay in Ne_2 *J. Phys.: Conf. Ser.* **4** 277
[111] Sisourat N, Kryzhevoi N V, Kolorenč P, Scheit S, Jahnke T and Cederbaum L S 2010 *Nat. Phys.* **6** 508